SISSA - SCUOLA INTERNAZIONALE SUPERIORE DI STUDI AVANZATI
TRIESTE
Strada Costiera 11

ISAS - INTERNATIONAL SCHOOL FOR ADVANCED STUDIES

FRACTALLY ROUGH SURFACES: WETTING, ADSORPTION AND SPECTRAL PROPERTIES

Thesis Submitted for Degree of:
Doctor Philosopiæ

Candidate:

Gilberto Giugliarelli

Supervisor:

Prof. Attilio L. Stella

Academic Year 1989/90

TRIESTE

This thesis is submitted for the degree of Doctor Phylosopiæin Biophysics. The content of the thesis is mainly devoted to the study of phenomena occurring or characterizing fractal surfaces. Under many points of view these topics can be considered part of statistical mechanics and phase transition fields. At some extent, however, the study of fractal surfaces and fractal properties has many contact points also with the structural and dynamical properties of biological and biophysical systems.

I started to be involved in the study of fractal concepts and in their application to the interpretation of real phenomena, in connection with the study of a specific biophysical problem for proteins. In fact, during the preparation of the Master Thesis, in this School in 1988, I worked, also from the experimental point of view, at a study in which fractal dynamics were used in order to relate the low frequency vibrational properties of some proteins with their geometrical self–similar structure. After that, it was then natural to continue the work on fractals and to extend my interest also to the physical phenomena considered in this thesis.

NOTES

Part of this thesis has been published and presented to congresses.

Publications:

- "Lattice–Gas Model for Adsorption on Fractally Rough Surfaces",
  G.Giugliarelli and A.L.Stella,
  Physica Scripta, (1990), in press.
- "Spectral Properties of Fractal Surfaces",
  G.Giugliarelli, A.Maritan and A.L.Stella,
  Europhysics Letters **11**, 101 (1990).

Invited Talks and Contributions to Conferences:

- "Lattice–Gas Model for Adsorption on Fractally Rough Surfaces",
  G.Giugliarelli and A.L.Stella,
  Invited Talk at:
  10th General Conference of the Condensed Matter Division of E.P.S., 9–12 April, 1990, Lisbon, Portugal
- "Lattice–Gas Model for Adsorption on Fractal Substrates",
  G.Giugliarelli and A.L.Stella,
  Invited Talk at:
  Meeting on "Phase Equilibria and Interfacial Phenomena", 10–11 May, 1990, Laboratorium voor Vaste Stof–Fysika en Magnetisme, Katholieke Universiteit Leuven, Belgium.
- "Lattice–Gas Model for Adsorption on Fractally Rough Surfaces",
  G.Giugliarelli and A.L.Stella,
  Conference on "Phase Transitions in Surface Films", Ettore Majorana Center, Erice, Italy, 19–30 June, 1990.
- "Spectral Properties of Fractal Surfaces",
  G.Giugliarelli, A.Maritan and A.L.Stella,
  10th General Conference of the Condensed Matter Division of E.P.S., 9–12 April, 1990, Lisbon, Portugal, Abstract Book p.171.

TABLE OF CONTENTS

Introduction 1

Part One 5

1. Adsorption and Wetting Phenomena 7

1.1 General Aspects 7

1.2 Lattice–Gas Models 11

1.2.1 Lattice–Gas Models with Short–Range Interactions . . 12

1.2.2 Lattice–Gas Models with Long–Range Interactions . . 13

1.3 Wetting in Non Standard Geometries 14

2. Surface Roughness and Adsorption Phenomena 17

2.1 Fractal Structures 18

2.1.1 Geometry of Fractal Structures 19

2.1.2 Dynamics of Fractal Structures 21

2.2 Study of Surface Geometry by Adsorption Techniques 23

2.3 A Survey oh Heuristic Arguments for Adsorption on Fractally Rough Substrates 25

2.3.1 De Gennes'Approach 25

2.3.2 Multilayer Adsorption on a Fractal Surface 28

2.3.3 Surface Tension Effects 31

2.4 Adsorption on Self–Affine Surfaces 32

2.5 Concluding Remarks 34

3. A Lattice–Gas Model for Wetting on Self–similar Surfaces 37

3.1 A Lattice–Gas Model for Adsorption on a Fractal Substrate . 37
3.1.1 The Model 38
3.1.2 Strategy Followed in the Calculations 42
3.1.3 The Substrate Potential and the Nature of the Isotherms 44
3.1.4 The Adsorption Isotherms: Low Coverage Regime . . 45
3.1.5 The Phase Diagram 48
3.1.6 Isotherms in the Multilayer Regime 49
3.2 Conclusions 53

Part Two 57

4. Fractal Surfaces, Random Walks and Self–Avoiding Walks 59
4.1 Spectral Properties of Fractal Surfaces 60
4.1.1 The problem 60
4.1.2 Computational Tools 62
4.1.3 Results and Discussion 62
4.1.4 A Scaling Argument 64
4.2 Implications for the Statistics of Polymeric Networks 66
4.3 The Random Chain 68
4.4 Self–Avoiding Walks 70
4.5 Conclusions 73

Bibliography 75
Acknowledgements 79

INTRODUCTION

In recent years the fractal paradigm [1] has became an important theoretical tool for the understanding of many physical issues involving complex and irregular structures. Applications of fractal concepts concern many different fields, like polymer statistics, [2] irreversible growth phenomena, [3] dynamical systems, [4] biophysics, [5] and others.

Fractal structures are characterized by dilation symmetries, or self–similarity, as opposed to more traditional symmetries, like translation invariance. From a theoretical point of view, this implies that many standard schemes have to be replaced by new approaches. So, e.g., in a solid state physics of fractal lattices, the renormalization group should somehow play the role of Bloch's theorem.

Structures in nature always posses self–similarity in a statistical sense and for a more or less wide range of length scales. The application of fractal models to physical phenomena is thus always subject to limitations, which should be carefully established in each case.

Fractal geometry can also be interpreted as a sort of hierarchical organization in the configuration space. In this respect the success of fractal ideas in physics could be seen as closely connected to the recent development of more general hierarchical ideas in fields like the statistical mechanics of spin glasses. [6]

In the present thesis we deal with a fractality which does not pertain to the bulk of the structures of interest, but just to their surface. Indeed we study physical phenomena occurring in the presence of self–similar surfaces delimiting otherwise regular and compact bulk regions (fat fractals). This kind of fractality, as a role, is more elusive and difficult to detect experimentally, than that involving

also the bulk of the structures. Nevertheless, fractal surfaces of the type just mentioned are expected to give rise to interesting phenomena, which could often differ substantially from the corresponding ones in more standard geometries. An understanding of these phenomena, besides being of much value in itself, could help in finding new ways of characterization of the geometry of the surfaces.

The phenomena we are dealing with in this thesis are adsorption and wetting, in Part One, and diffusion and spectral properties, in Part Two.

Compared to our present knowledge of wetting and adsorption in the case of flat substrates,[7] our understanding of the same processes on rough surfaces is extremely poor. This is a particularly unlucky situation, if we, e.g., consider that adsorption has been repeatedly proposed as one of the most natural and promising probes of fractality in rough substrates.[9–11]

In Part One of the thesis we report a contribution, which is intended to fill, to a limited extent, the gap of our knowledge in this field. In particular, we present the first statistical mechanical treatment of a lattice–gas model, which, albeit qualitatively, should contain all the main physical ingredients for the explanation of adsorption on fractal surfaces. The (mean field) solution of this model gives a full thermodynamic description of the phenomenon, and allows to discuss critically previous conjectures[10–11] about the scalings involved in it. We believe that with some additional efforts and extensions, the type of model analysis carried out here could be of substantial help in clarifying controversial issues like the interpretation of recent experiments on multilayer adsorption.[10]

In Part Two we address another extensive model calculation. This time we deal with the spectral properties of fractal surfaces, as revealed by the diffusion processes occurring on them.

Since the pioneering works of Alexander and Orbach[12] and Rammal and Toulouse[13] an extensive literature has developed about the dynamics of fractal structures. On the other hand, to our knowledge, a calculation, like that undertaken in this thesis for a model fractal surface, was never performed before.

The spectral dimension of a fractal surface can be experimentally determined, e.g., by means of neutron scattering techniques.[14] On the other hand, we think that further important motivations for a study like our one, are given by the

interesting connections one can establish between spectral properties and issues, like the conformational statistics of hierarchical polymeric networks, random and self–avoiding chains and Flory approximations on fractal structures, which are all discussed in Part Two.

The thesis is organized as follows.

In Chapter 1 of Part One we give some introduction to wetting phenomena in standard geometries and to their lattice–gas model description.

An elementary introduction to some basic concepts of fractal geometry and fractal dynamics is given in Chapter 2. In this chapter a review of heuristic and phenomenological approaches to wetting and adsorption on fractal and self–affine substrates is presented.

Chapter 3 is devoted to a presentation of our lattice–gas model for adsorption on fractal substrates and to its mean field solution.

Chapter 4 in Part Two discusses the spectral and diffusion dimensions of a model of fractal surface (hydrant) and of the related issues mentioned above.

PART
ONE

CHAPTER 1

ADSORPTION AND WETTING PHENOMENA

The formation of liquid drops on a surface is a rather common phenomenon. The interest of physicists for this phenomenon is related to the connections existing between the macroscopic shape of the drop and the three surface tensions associated with the three interfaces meeting at the contact line between the drop and the substrate. The contact angle Θ (see Fig. 1.1) gives the possibility to make an easy classification for the wettability of the substrate by an adsorbate: a wet substrate will be obtained when $\Theta = 0$, a non–wet substrate when $\Theta < \pi$ and finally a dry substrate when $\Theta = \pi$. Because of the dependence of Θ on the various surface tensions, it is obvious that its value changes, e.g., with a change in chemical composition of the liquid drop, or with temperature, etc...

In this thesis we are not interested to examine all the cases of the contact angle Θ. We shall restrict ourselves to consider wet substrates ($\Theta = 0$) in the case of non standard geometries. In this chapter we want to give first a summary of the concepts and the theoretical methods for the study of adsorption and wetting phenomena on flat and in general smooth surfaces.

1.1 GENERAL ASPECTS

The formation of a liquid layer near a wall is the phenomenon on which we

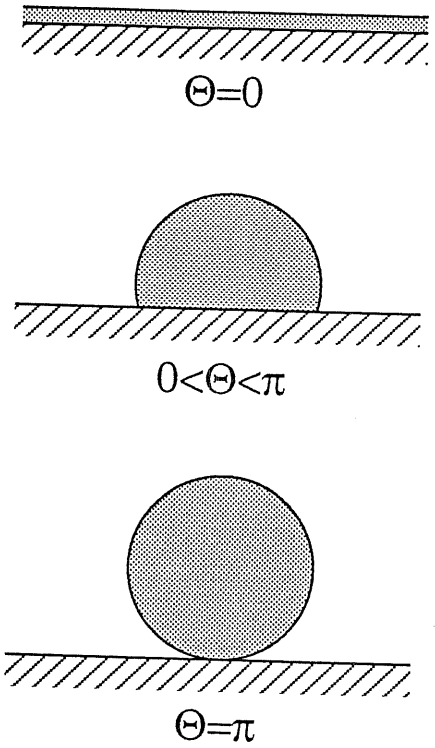

Fig. 1.1 Wet (Θ=0), non–wet ($0<\Theta<\pi$), and dry ($\Theta=\pi$) substrates. In the non–wet case a microscopic liquid layer covers that part of the substrate that is not beneath the drop. Note that this thin layer is missing for a dry substrate.

want to concentrate our attention here. The knowledge of the dependence of the liquid density ρ on coordinates and on the relevant thermodynamic parameters would give a complete insight into the physics of this phenomenon. However, for many issues one does not need a detailed description of ρ. Often the knowledge of the excess density or coverage ρ_s is sufficient. This quantity is related to the density ρ by the following equation:[7]

$$\rho_s = \int_0^\infty dz[\rho(z) - \rho(\infty)], \tag{1.1}$$

which can be further simplified in the case of T not too close to T_c. In fact, because of the sudden decrease of the density around $z = l$, (see Fig. 1.2) ρ_s is proportional to l

$$\rho_s \cong (\rho_l - \rho_g)l \tag{1.2}$$

Thus the study of wetting of substrates concerns the dependence of ρ_s on μ

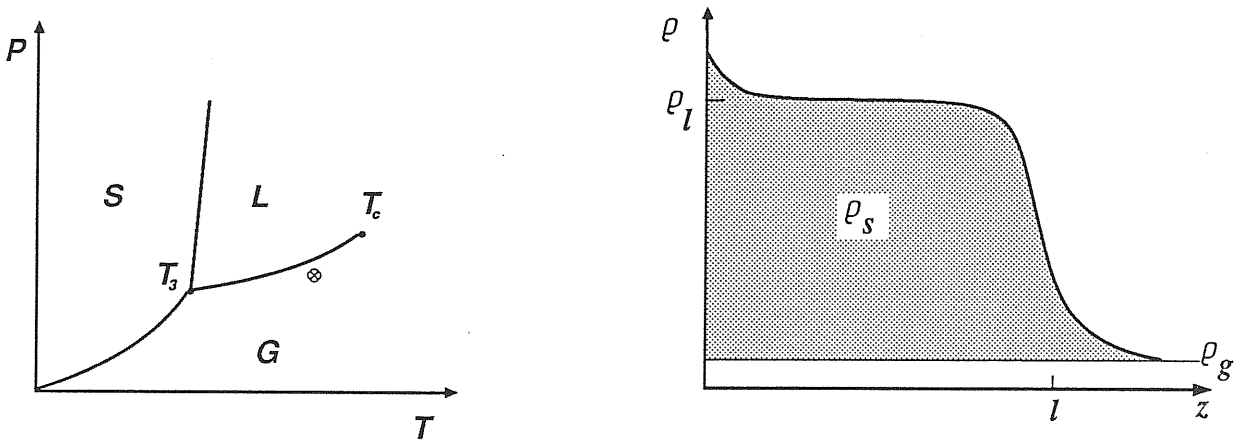

Fig. 1.2 Generic phase diagram in pressure–temperature variables for a one–component system with solid, liquid and gas phases. The melting– and sublimation–lines meet the gas–liquid coexistence line at the triple point T_3. The gas–liquid coexistence line ends at the critical point T_c. $\otimes$ denotes a typical equilibrium situation leading to a density profile $\rho(z)$ as in *b*). *b*) The density profile $\rho(z)$ of a gas close to a substrate; ρ_s denotes the coverage of the substrate. For simplicity, density oscillations close to the substrate, occurring owing to packing effects, are suppressed. The system is assumed to be homogeneous parallel to the surface, so that ρ depends only on z.

and T (chemical potential and temperature, respectively), as well as on adparticle–adparticle interactions and substrate potential.

In order to set up a vocabulary for wetting phenomena, let us first consider the phase diagram of Fig. 1.2 and suppose to be in the neighbourhood of the gas–liquid coexistence line, By letting $\mu \to \mu_0^-$ (μ_0 being the value of the chemical potential at coexistence) we could observe that, for $T < T_w$, $\rho_s(\mu_0^-)$ remains finite, while for any $T \geq T_w$, $\rho_s(\mu_0^-)$ diverges. In this case the phenomenon occurring above T_w is called *complete wetting* and T_w *wetting temperature*. This change in behaviour when temperature is lower or higher than T_w has to be considered as a transition, i.e. *wetting transition*. To establish the order of this transition we can consider a path, in the phase diagram of Fig. 1.2, at $\mu = \mu_0^-$. If ρ_s diverges smoothly when $T \to T_w$, we can talk of a *second order wetting transition* or equivalently *critical wetting*; otherwise, if the coverage jumps from a finite value at T_w^- to an infinite value at T_w^+, we can talk of a *first order wetting transition*. In general the order of the wetting transition depends on the balance between the interaction between adparticles and the substrate potential. A slight modification, e.g., in the

substrate potential, can change the order of the wetting transition.

With reference to Fig. 1.2, let us now imagine to be in the neighbourhood of the sublimation line (gas–solid coexistence line). In this conditions it is usual to observe that a solid–like film condenses on the substrate. A common feature of this phenomenon is the so called *layering*; one can distinguish whether a monolayer, or two layers, etc., are formed. Usually, completion of each layer is accompanied by a first order transition revealed by a discontinuous jump in coverage. The lines where this singularities occur end at critical points. The critical points of the layer transition from layer n to $n+1$, $T_{c,n}$, accumulate at T_R, the *roughening temperature.*[15,16] This is the temperature at which the amplitude of the fluctuations in the adsorbed layers become predominant with respect to the growing up of the film and the transitions between the layers are washed out.

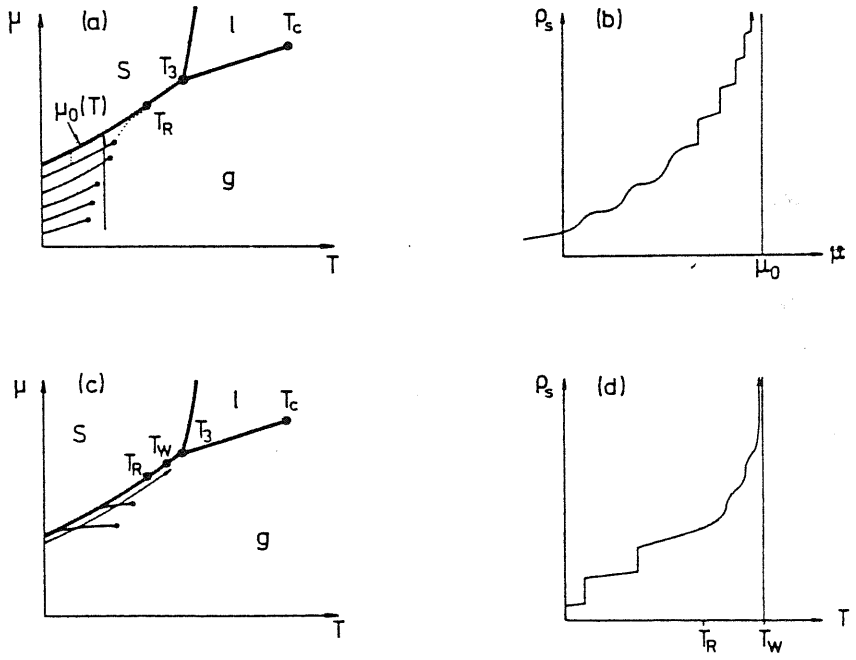

Fig. 1.3 Wetting phenomena along the sublimation curve. (*a*) A system with T_w=0 and a corresponding adsorption isotherm, (*b*). (*c*) A system that is non–wet at T=0 with the roughening temperature T_R below the wetting temperature. (*d*) A sketch of the coverage for a path at μ_0^- in (*c*). Further details are given in the main text.

1.2 LATTICE–GAS MODELS

The study of wetting problems has been approached essentially in two different ways. One is the analysis of lattice–gas models or density– functional theories in a semi–infinite geometry in which a substrate potential acts on the particles. The other consists in using an effective interface potential and in studying the depinning of this interface in terms of a Landau–type continuum theory. Here we are interested in giving a summary of the lattice–gas models and their features in view of the original developments to be reported in Chapter 3 for the case of substrates with fractal surface.

Lattice–gas models are based on the idea of substituting the three–dimensional world with a regular lattice. The particles of the system can occupy only the lattice sites and to each site an occupation number $n_i = 0, 1$ remains associated . In order to apply the lattice–gas model to the study of wetting phenomena, some other ingredients have to be included. For wetting of a flat substrate, it is common to consider a lattice filling the half–space $z > 0$. This portion of space is under the influence of a potential due to the solid substrate in the $z < 0$ region. In general, we can write the Hamiltonian of this system as follows

$$\mathcal{H} = \sum_i V_i n_i + \frac{1}{2} \sum_{ij} w_{ij} n_i n_j \tag{1.3}$$

Here, V is the substrate potential while w is the interaction potential between the gas particles. The sums are done over all the lattice sites.

Starting from this Hamiltonian, one can use different methods to solve the problem of wetting. One of the most widely used is the mean field (MF) approximation. To this purpose is better to write the free energy of the system in the grand canonical ensemble. In the MF approximation the occupation numbers n_i have to be substituted by their average values ρ_i which enter in the free energy functional:

$$\mathcal{F} = \sum_i \{k_B T[\rho_i \ln \rho_i + (1 - \rho_i) \ln(1 - \rho_i)] + (V_i - \mu)\rho_i\} + \frac{1}{2} \sum_{ij} w_{ij} \rho_i \rho_j \tag{1.4}$$

The solution of the problem, i.e., the determination of the free energy at given μ and T, consists in finding the global minimum of (1.4) for those μ and T. The

stationary conditions $\partial\mathcal{F}/\partial\rho_k = 0$ leads to the mean–field equations,

$$\rho_k = \left[1 + e^{(V_k + \sum_i w_{ki}\rho_i - \mu)/k_B T}\right]^{-1} \tag{1.5}$$

These equations can be solved by iteration with appropriate boundary conditions. The coverage ρ_s at a given μ and T can be obtained now as

$$\rho_s(\mu, T) = \sum_i [\rho_i^*(\mu, T) - \rho_b(\mu, T)] \tag{1.6}$$

where $\rho_b(\mu, T)$ is bulk value of the low density phase and the ρ^*'s constitute the solution of (1.5).

1.2.1 *LATTICE–GAS MODELS WITH SHORT–RANGE INTERACTIONS*

With few exceptions, lattice–gas models for the description of wetting phenomena, for simplicity include only nearest–neighbour adparticle–adparticle interactions. In spite of their schematic characterization, such models display the whole variety of surface phase diagrams as discussed in the previous section. E.g., Pandit *et al.* studied explicitly within the MF approximation a lattice–gas model characterized by nearest–neighbour adparticle–adparticle interaction of strength v.[17] The substrate exerts potential of strength u on adsorbate particles in the layer just next to the substrate. For $(u/v) > 1$, the substrate is so strong that it is already wet at $T = 0$ ($T_w = 0$). One finds a wetting transition ($T_w > 0$) for $0.7 < (u/v) < 0.9$; in this case the transition is of the first order. For lower values of (u/v) ($0.5 < (u/v) < 0.7$) one has critical wetting. For $0 < (u/v) < 0.5$ the corresponding drying transition occurs. In the parameter region $0.9 < (u/v) < 1$ one finds both wetting transition and (as for $(u/v) \geq 1$) layering transitions. This fact needs some comments. Layering transitions should occur only along the sublimation line (as mentioned in the previous section) or along the melting curve. However, this lattice–gas model describes the liquid–gas transition; its coexistence line ends at a critical point T_c and not at a triple–point T_3 (the three–phase coexistence point). As a consequence, these layering transitions have to be regarded as a shortcoming of the lattice–gas model, because it describes gas–liquid coexistence. Nevertheless, they look strikingly similar to what is observed experimentally along the sublimation line.

Other lattice–gas models based on short range interactions were used[18] to argue that, in spite of the missing triple–point T_3, the surface behaviour along the sublimation and gas–liquid coexistence lines, as long as T_c is not to close to T_3, is correctly described. More sofisticated versions of lattice–gas models include that discussed by Ebner (see ref. [19]), based on the six–state Potts model with vacancies. In this model one can identify three different phases meeting at a triple–point. By the analysis of this model Ebner found interesting wetting phenomena which later were also found experimentally.[20]

Lattice–gas models have several advantages with respect to other theoretical schematizations. They allow the study of effects on an atomic scale. Moreover, they constitute a natural framework for the investigation of fluctuation effects via Monte Carlo techniques.

1.2.2 *LATTICE–GAS MODELS WITH LONG–RANGE INTERACTIONS*

As said above, models with short–range interactions display a rich variety of wetting behaviours. However, it is well established that for real liquids the interaction potential between particles at distance r is van der Waals–like, i.e. $w(r) \propto r^{-6}$ for large r. On the other hand, the substrate potential has a similar nature and, taking into account the contribute of all the substrate atoms, it is of the type $V(z) \propto z^{-3}$, if z is the distance from the substrate.

The van der Waals tail of the liquid–liquid interaction is almost irrelevant for the critical behaviour of many liquids; this is essentially the reason why they have the same critical behaviour as the three–dimensional Ising model. However, because wetting transition occur below T_c, one cannot expect that the rules valid in the bulk phase remain valid also in the case of surface critical phenomena. It is interesting, on the other hand, to notice that near T_c wetting phenomena, as, e.g., complete wetting at T_c, long–range adparticle–adparticle interactions become irrelevant. The tail of the substrate potential is essential, in any case, to reproduce the asymptotic behaviour of the adsorption isotherms found also experimentally.

In the literature are several examples of lattice-gas models in which long–range interactions have been included. De Oliveira and Griffiths (see ref. [21]) and Ebner (see ref. [22]) have studied lattice–gas models in which nearest–neighbour liquid–

liquid interaction and long–range substrate potential ($V(z) \propto z^{-3}$) were considered. These models together with others [23–26] were always solved numerically by MF approximation. In spite of the fact that for models with both short–range and long–range interaction , one finds similar features (presence of wetting transition, critical temperatures, layering, etc...), the correct asymptotic scaling of the relevant quantities in wetting is found only in the latter case. For example, models with long–range interactions, at least for the substrate potential, correctly reproduce the asymptotic behaviour of the adsorption isotherms. The coverage, follows the relation:

$$\rho_s \propto (\mu_0 - \mu)^{-1/3} \tag{1.7}$$

which is essentially a consequence of the scaling of the substrate potential V with distance.

1.3 WETTING IN NON STANDARD GEOMETRIES

The systems discussed in the previous sections have always the feature of having flat or smooth substrate surfaces. There are, however, other interesting situations in which the geometry is more confined or in which the interfaces are curved. Examples of these are porous media, [27] rough surfaces, colloidal suspensions, etc....

Let us consider a simple situation which differs only slightly from the flat case treated so far. A gas is confined between two planar plates at distance L from each other. As $L \to \infty$ one recovers the discussed flat case. Because of the confined situation, it is expected that the chemical potential $\mu_b(L)$, at which complete filling of the space between the two plates takes place, should be shifted at lower values with respect to μ_0. At $\mu_b(L)$, in the capillary, the gas undergoes a first–order condensation into a liquid–like before the bulk coexistence is reached. This phenomenon is called *capillary condensation.* The relation between $\mu_b(L)$ and μ_0, using the Kelvin equation, can be written as: [23–30]

$$\mu_b(L) = \mu_0 - 2\sigma_{g,l}(\rho_l - \rho_g)^{-1}L^{-1} \tag{1.8}$$

A wetting layer grows with a thickness $l = [2a/(\rho_l - \rho_g)]^{1/3}(\mu_0 - \mu)^{-1/3}$, [7] in the

case of an infinite wall separation ($L \to \infty$). For finite L the above l grows up to a finite value, l_{max}, after which suddenly the liquid fills the space between the planes. By eq.(1.8), it is possible to see that this quantity behaves like:

$$l_{max} = (a/\sigma_{g,l})^{1/3} L^{1/3} \tag{1.9}$$

Capillary condensation is not only a phenomenon arising in confined geometries. When the geometry is not planar capillary condensation influences wetting and competes with it. E.g., in a system in which pores are present on a flat substrate, effects similar to those summarized above are observed. In this case, the occurrence of capillary condensation does not change the asymptotic behaviour of the wetting phenomenon; however, at the pore level, a filling process will take place with features qualitatively analogous to those mentioned above. The shape of the pore will, of course, influence the capillary condensation, determining the rapidity of the "pore–filling" phenomenon.

Wetting of curved substrates also displays interesting features. Since for them an increase of the thickness of the adsorbed layer changes the area of the interface, the free energy of the system will depend also on the curvature of the surface it self. Let us consider, e.g., cylindrical or spherical surfaces. The curvature effects increase the thickness of the wetted layer at the inner surfaces. Anyway, for a cylinder (sphere) of radius R, because of the finite–size effects, the system exhibits no phase transition. However, for large R the corresponding sudden rise region of, e.g., the coverage, becomes very narrow and a (pseudo)–transition point can be defined.

On the contrary, for wetting at the outer surfaces, the curvature effects prevent the build–up of a thick layer, even at coexistence between gas and liquid. In this case, there exists an upper limit for the thickness of the film after that the growth of the film is no more possible.

From these last considerations one can suspect that curvature effects should be particularly important in porous media and in rough surfaces. For many years, there have been many attempts to estimate the inner surface area of porous materials[27,31] and, more recently of rough and fractal surfaces[8,9] by means of adsorption techniques. However, up to now only rough estimates have been obtained.

CHAPTER 2

SURFACE ROUGHNESS AND ADSORPTION PHENOMENA

Wetting of solid surfaces by liquids has many practical applications and has been an important area of both basic and applied research for many years. However, many of the most complicated "real" wetting and adsorption processes are still, at best, only partially understood. In particular, we have a relatively poor understanding of wetting in the vicinity of a rough substrate. The reason for this is the fact that, in general, theoretical schemes for the understanding of wetting on flat substrates, completely fail when applied to rough surfaces.

From the geometrical point of view, rough surfaces can be characterized in different ways, depending on the nature of the material. In particular, as mentioned in the Introduction of this thesis, fractal geometry and self–similarity have often shown to be suitable for their description. It is remarkable that, e.g., solid surfaces of carbonaceous materials reveal fractality by means of several different experimental techniques (e.g., adsorption studies, analysis of small angle X–ray and neutron scattering data, porosimetry, etc...) (see Ref. [32] and references therein). On the other hand, also for some biological systems a description in terms of fractal geometry seems to be appropriate. In particular, it was shown [33] that the surface of some proteins, as revealed by X–ray diffraction determination of the atom coordinates, displays clear fractal features. In view of such evidences, it is extremely interesting to study the properties of wetting phenomena taking place in fractal environments.

It is legitimate to think that these phenomena should have peculiar features that could be radically different from those in usual environments. Another source of interest comes from the fact that, surprisingly enough, in the recent literature years adsorption experiments were extensively used to get information on the fractality of material surfaces.

Here, we would like to give a short review of the experimental facts about adsorption on rough surfaces and of some of the main theoretical arguments proposed recently to interpret the experimental data.

Since in the discussion we will make extensive use of concepts like self–similarity and fractality, we start by giving an elementary introduction to these concepts.

2.1 FRACTAL STRUCTURES

Fractal concepts were originally developed by mathematicians about a century ago, under the influence of a crisis in mathematics. The divulgation among physicists of these geometrical ideas, and the term "fractals", is due to B. Mandelbrot [1]. To introduce the main ideas concerning fractal objects it is instructive to give first an example from the physics of critical phenomena. It is well known that a fluid near its critical point, because of strong fluctuations, is a mixture of gas and liquid droplets. In fact, looking more carefully, one could observe that, as the critical point is approached more closely, each liquid droplet contains small vapor droplets which again contain smaller liquid droplets, etc... We can say that the system does not show a characteristic length scale and we can find parts of the system that look very similar to larger parts of the whole system, provided an appropriate rescaling is performed. This property is called self–similarity and constitutes a general feature of fractal objects. Looking at a fractal structure, we can find, at different length scales portions of the structure itself, which, upon proper rescaling, look almost identical.

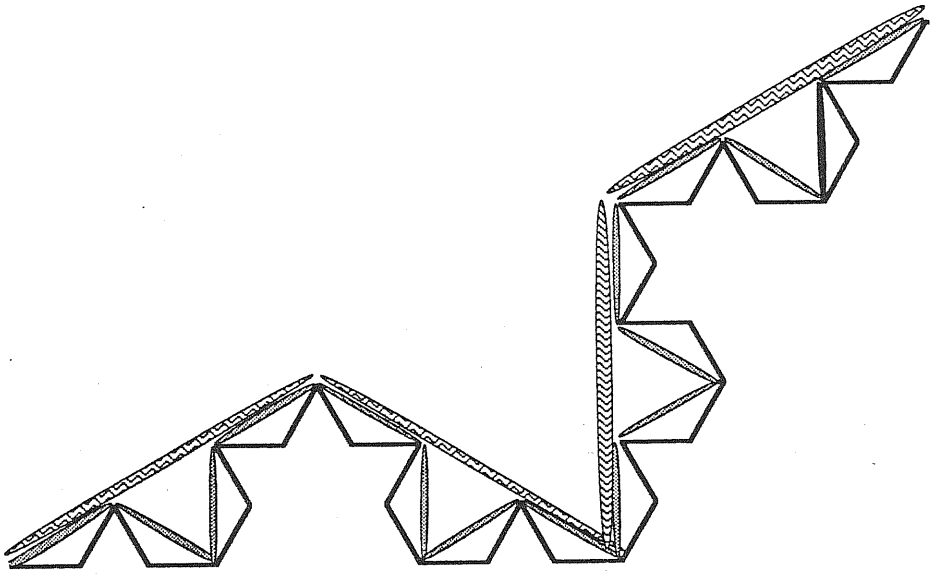

Fig. 2.1 Measure of the length of a fractal curve (Koch curve in the figure) by using yardsticks of different lengths. The curve have clearly a fractal dimension $\bar{d}$=ln 4 / ln 3.

2.1.1 *GEOMETRY OF FRACTAL STRUCTURES*

Fractal objects are characterized by dimensions. If we, e.g., consider the volume $\mathcal{V}$ effectively occupied (or the mass $\mathcal{M}$) by the portion of a fractal structure inside a sphere of radius R, we obtain that

$$\mathcal{V} \propto R^{\bar{d}}, \tag{2.1}$$

Where $\bar{d}$ is the so called fractal or capacity dimension. This dimension characterizes the scaling of the volume (mass) of the fractal structure with the size of the region one considers. Eq. (2.1) can also be considered as the generalization of the relation $\mathcal{V} \propto R^d$ valid for compact and homogeneous objects. For fractals $\bar{d}$ assumes generally non–integer values.

Another way to clarify the meaning of fractality of a given structure, is the following. Let us consider the situation in Fig. 2.1. Here we are trying to measure the "length" L of a fractal curve using yardsticks of different lengths. In this case, the measured length will be given by the number of yardsticks of a certain length,

needed to cover the curve, times the yardstick length l. For a fractal curve (as in Fig. 2.1) the length will scale as

$$L \propto l^{\bar{d}} \tag{2.2}$$

where $\bar{d}$ is also in this case the fractal dimension of the structure. Similarly, in the case of a fractal surface, one could define the surface fractal dimension $\bar{d}$ as the scaling exponent of the measured surface area, as a function of the linear size of, e.g., disquettes used to cover the surface.

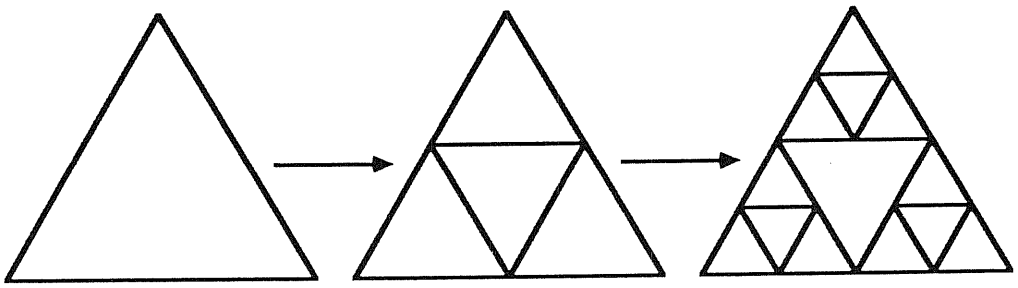

Fig. 2.2 Sierpinski Gasket ($\bar{d}$=ln 3 / ln 2).

Geometrically fractal structures can be constructed by the application of recursive laws. As sketched in Fig. 2.2, one obtains a deterministic fractal, i.e., a Sierpinski Gasket, recursively, by applying a transformation law to a simple starting geometrical object. In this case, the self–similarity of the resulting object, provided that an infinite system is obtained, holds by construction. In Fig. 2.3 is reported another example of deterministic fractal.

In nature, one finds often systems with fractal properties. Self–similarity and fractality, in these cases, are only properties holding on a statistical base. This means that, e.g., a definition of the fractal dimension $\bar{d}$ is possible only by considering some kind of ensemble averages. Notable examples are the incipient infinite percolation cluster, the droplets of the Ising model, the random walk, linear polymers, etc... For a random walk (RW) of N steps in d-dimensional space, the average end-to-end distance is given by

$$\langle R \rangle \propto N^{1/2} \equiv N^{1/d_w} \tag{2.3}$$

with $d_w = 2$ when $d \geq 2$. Since $\langle R \rangle$ represents the average extension of the ensemble of points of a RW of N steps, we can conclude that d_w is the RW fractal dimension ($N \propto \langle R \rangle^{d_w}$). When RWs on a fractal structure are considered, the value of d_w can be considerably different from 2. We will discuss an example of this in Chapter 4.

Another example of random fractal model, which reproduces very well the conformational properties of real linear polymers in "good" solvents, is the self-avoiding walk (SAW). In this case only walks without overlaps or intersections are allowed. For SAWs one finds

$$\langle R \rangle \propto N^{\nu} \equiv N^{1/d_{SAW}}, \tag{2.4}$$

where on regular lattices, d_{SAW} is a function of dimensionality d, and $d_{SAW}(d) < 2$ for $d < 4$. In a two-dimensional space d_{SAW} is found to be $4/3$,[34], while in three dimensions, a value of d_{SAW} close to $5/3$ has been found.

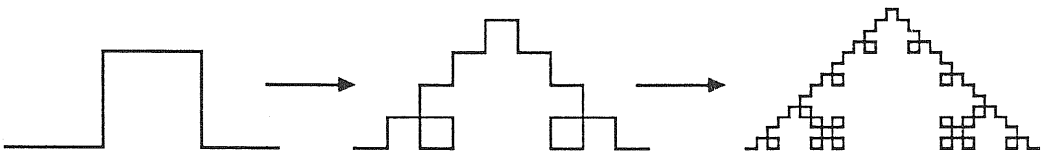

Fig. 2.3 A deterministic fractal with $\bar{d}$=ln 3/ln2.

2.1.2 *DYNAMICS OF FRACTAL STRUCTURES*

The dynamical properties of fractal structures are of much interest for several physical problems. De Gennes was the first to address the study of a dynamical process on a fractal structure (the ant in the labyrinth).[35] More recently problems of this kind were considered also in connection with the ambitious program of understanding anomalous relaxation properties of biopolymers by Stapleton and co-workers and by Alexander and Orbach.[5,12]

Elastic vibrations of a structure can be schematically studied in terms of an equation of the following type

$$m_i \frac{d^2 u_i}{dt^2} = \sum_j K_{ij}(u_j - u_i) \tag{2.5}$$

where u_i is the displacement from the equilibrium position of the i–th particle of the structure, m_i is its mass and K_{ij} is the elastic constant of the "spring" connecting particles i and j. Solution of this equation give rise to the normal modes picture of the elastic vibrations. For homogeneous structures, from such an analysis one obtains the well known result, that the density of vibrational modes, $\rho(\omega)$, scales, in the limit of low frequency, as

$$\rho(\omega) \propto \omega^{d-1} \qquad (\omega \to 0) \tag{2.6}$$

where d is the euclidean dimension of the system. For a fractal structure it was realized that a straightforward generalization of eq. (2.6), with $\bar{d}$ replacing d, does not hold. Indeed, the law replacing (2.6) for a fractal involves a new dimension.

To introduce this important quantity, it is better to consider an alternative way method to gain information on the vibrational modes of a structure. This consists in solving first the diffusion problem on the structure. One substitutes the elastic spring connecting two points of the structure with a jumping rate, for a diffusing particle, of strength proportional to the corresponding K. In such way one obtains a relation between the probability functions, solutions of the diffusion problem, and the density of the vibrational states. Indeed, if $P_0(t)$ is the probability of finding a diffusing particle at the starting point, 0, at time t, one easily finds [12]

$$\rho(\omega) = \frac{2\omega}{\pi} Im\langle \tilde{P}_0(-\omega^2 + i0^+), \rangle \tag{2.7}$$

where an average over all possible starting points has been considered. In eq. (2.7) $\tilde{P}_0(\epsilon)$ is the Laplace transform of $P_0(t)$:

$$\tilde{P}_0(\epsilon) = \int_0^\infty dt e^{-\epsilon t} P_0(t) \tag{2.8}$$

For a fractal structure, $P_0(t)$ is expected to scale as the inverse of the number of distinct points visited on the structure in time t, $S(t)$, thus

$$P_0(t) \propto S^{-1}(t) \propto R^{-\bar{d}} \propto t^{-\bar{d}/d_w} \qquad (t \to \infty) \tag{2.9}$$

The Laplace transform of this equation gives

$$\tilde{P}_0(\epsilon) \propto \epsilon^{\frac{\bar{d}}{d_w}-1} \qquad (\epsilon \to 0) \tag{2.10}$$

and finally from eq. (2.7)

$$\rho(\omega) \propto \omega \cdot \omega^{2\frac{\bar{d}}{d_w}-2} = \omega^{2\frac{\bar{d}}{d_w}-1} \equiv \omega^{\tilde{d}-1}. \tag{2.11}$$

$\tilde{d} = 2\bar{d}/d_w$, first introduced by Alexander and Orbach (see ref. [12]), is the so called spectral or fracton dimension. Eq. (2.11) shows that, as far as the density of vibrational states in the low frequency limit is concerned, fractal structures exhibit a $\rho(\omega)$ scaling in a way similar to that of the homogeneous systems. However, the spectral dimension $\tilde{d}$ is not only a parameter depending on geometrical features of the structure, but contains also dynamical ingredients. In general, modifications of the range and connectivity of the forces between different points of the system can strongly influence the value of the corresponding $\tilde{d}$, without implying any change of $\bar{d}$.[36]

2.2 STUDY OF SURFACE GEOMETRY BY ADSORPTION TECHNIQUES

There are several experimental facts justifying interest in adsorption on rough surfaces. In fact, isotherms can provide a double insight: a) these should characterize the wetting phenomena taking place in the vicinity of a rough substrate; b) the analysis of the data could be used to infer the possible geometrical scaling properties of the substrate surfaces.

Indeed, monolayer adsorption of many different gases on material surfaces was proposed[8] as a method for the determination of their surface fractal dimension. This is based on the fact that in the case of a self–similar surface, the number, N_m, of molecules required to cover the surface with a monolayer scales with molecule size, a, as (see also previous section)

$$N_m \propto a^{-\bar{d}} \tag{2.12}$$

This is a peculiar property of self–similar surfaces ($\overline{d}$ should have values in the range $2 < \overline{d} < 3$). For a variety of rock surfaces, the analysis of monolayer adsorption data referring to molecules of different sizes has shown that often N_m scales in a way apparently consistent with that of eq.(2.12), with $\overline{d}$ in the expected range.[8]

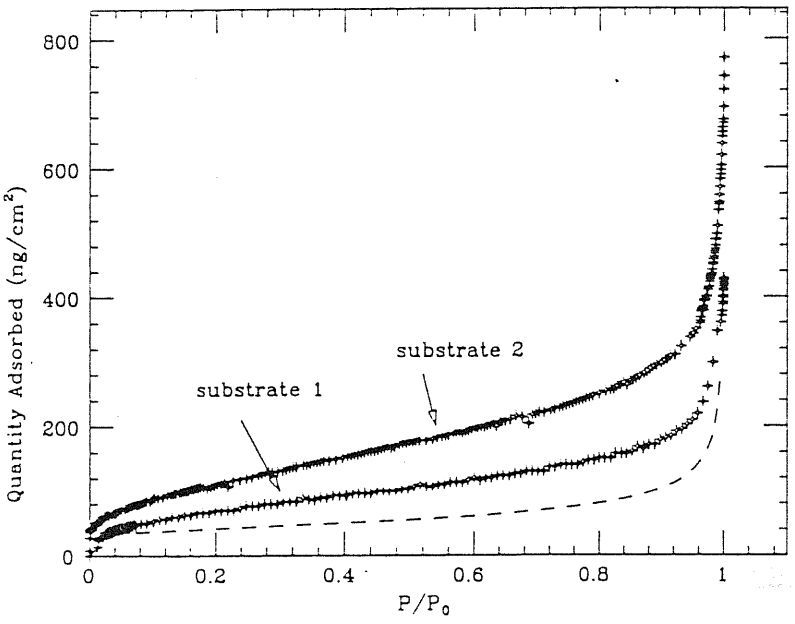

Fig. 2.4 Adsorption data for N_2 on two rough Ag substrates at 77 K. The substrate consists of electron–beam evaporated silver on quartz. In the figure is reported the quantity adsorbed in units of ng/cm^2 and the reference area is the macroscopic surface area of the electrode, i.e., the area of a hypothetical planar deposit. The dashed line shows the isotherm calculated for a flat surface. (From ref. [10])

More recently Pfeifer et al.[10] reported some experimental data about adsorption of N_2 on two rough Ag substrates at 77 K(see Fig. 2.4). On the basis of phenomenological considerations (see sect. 2.3.2) they suggested that also the multilayer adsorption (i.e. adsorption isotherms in the high coverage regime) could give informations on the surface fractality of the surfaces. However, the same set of experimental data was also interpreted in terms of a different theoretical approach (see sect. 2.4) in which adsorption is considered to take place on a self–affine surface.[37] It is also important to note, however, that the behaviour of the ad-

sorption isotherms reported in Fig. 2.4 is not obtained with the majority of the samples. Indeed, with *Ag* rough substrates obtained in ways very similar to those mentioned above, often the isotherms display different behaviours in such a way that, also in the high coverage regime, a power law is no more legitimated.[38] This circumstance can probably be related to the strong hysteresis found in those experiments.

From what reported above, it should be clear that there is not yet a general agreement on the interpretation of experimental data of adsorption on rough surfaces. Indeed at present, a satisfactory description of how fractality, self–affinity and, in general, surface roughness influence and determine the features of adsorption and wetting phenomenon does not exist yet.

2.3 A SURVEY OF HEURISTIC ARGUMENTS FOR ADSORPTION ON FRACTALLY ROUGH SUBSTRATES

There have been many attempts, in the last years, to build–up models for wetting and adsorption on rough substrates. In particular, for those substrates displaying fractal properties there are phenomenological approaches to be reported below. All these approaches are based on schematic and often oversimplified modellizations of the substrate surface and, because of the continuum nature of the description they provide, can be applied only to the multilayer regime. By these models one can estimate the scaling properties of quantities as coverage and film thickness.

2.3.1 *DE GENNES' APPROACH*[9]

De Gennes was the first to approach the problem of wetting on fractal surfaces. He considered substrates with a surface, which, in a range $l_1 < l < l_2$ (typical values for l_1 and l_2 could be $l_1 = 100\mathring{A}$ and $l_2 = 100\mu m$), has the property that the volume occupied (in a grain of size l_2) by void space at a minimal distance $\leq r$ from the surface scales as

$$\Omega(r) \propto l_2^{\bar{d}} \; r^{3-\bar{d}} \tag{2.13}$$

This equation, with 3 replaced by d, in fact express a property of all surfaces with fractal dimension $\bar{d}$ delimiting bulk regions with the dimension,d, of the embedding space.

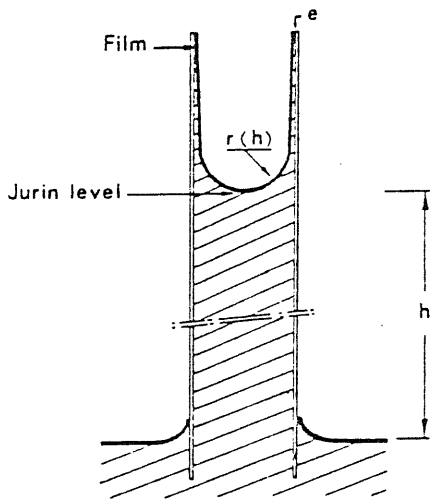

Fig. 2.5 Imbibition of a vertical capillary by a wetting fluid

De Gennes considered as a starting point the case in which a macroscopic capillary is filled up by a wetting fluid (see Fig.2.5). Using Young–Laplace law, one obtains that the capillary will be filled up to a level h satisfying the equation

$$p = \rho g h = 2\gamma / r \tag{2.14}$$

where γ is the surface tension of the fluid and r is the radius of curvature of the meniscus of the liquid in the capillary. This equation defines the function $r(p)$ which is essential for what follows.

If one considers now a pore whose shape differs from that of the cylindrical capillary of Fig. 2.5 , eq. (2.14) should be slightly refined. However, de Gennes notes that the volume of wetting liquid should have a behaviour similar to that mentioned above should. In this, case the wetting fluid will fill partly the pore in such a way that the radius of curvature of the film surface will be equal to $r(p)$, as expressed by eq. (2.14). In general, the volume of the fluid in a pore will scale as

$$\Omega_1 = \mathcal{V} f(R/r) \tag{2.15}$$

where $\mathcal{V}$ is the volume of the pore and R its characteristic length scale (see for example Fig. 2.6). $f(u)$ is of the order of unity for $u = 0$, and vanishes for $u = 1$. This function controls the filling up of the pore.

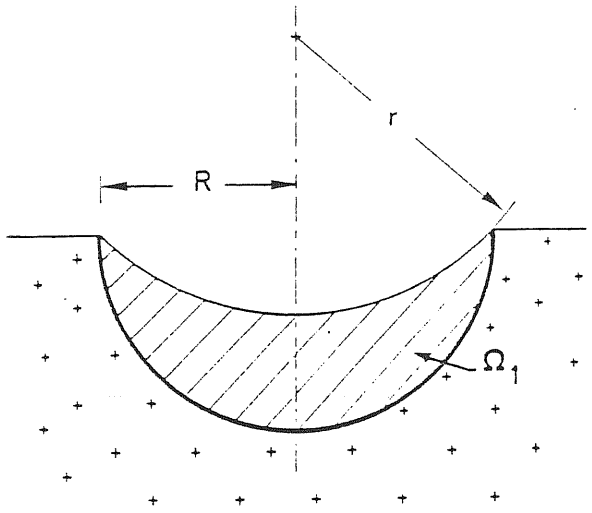

Fig. 2.6 Partial filling of a single hemispherical pore

Let us consider now two examples of systems with a fractal surface (see Fig. 2.7). In the case of iterative pits (Fig. 2.7*a*), if $\overline{d}$ is the fractal dimension of the surface, from eq. (2.13), the total volume of all pits of radius $\leq R$ (inside a volume l_2^3 of porous material) is $\Omega_0(R) \propto l_2^{\overline{d}} R^{3-\overline{d}}$. So the volume of liquid in these pits, at a certain pressure p, is

$$\Omega(r(p)) = \int_{l_1}^{r(p)} \frac{d\Omega_0}{dR} dR f(R/r(p)) \tag{2.16}$$

By changing variables from R to $u = R/r$ one easily obtains

$$\Omega(r) \propto l_2^{\overline{d}} r^{3-\overline{d}} \tag{2.17}$$

and the ratio between the volume of the wetting liquid, ϕ_L, and that of the pores, ϕ, is given by

$$\phi_L/\phi \sim (r/l_2)^{3-\overline{d}} \tag{2.18}$$

This equation is the central result of de Gennes' approach. With similar arguments it is possible to show that also in the case of "iterative flocs" (Fig.2.7*b*) one has the same scaling relation between the volume of the wetting liquid and

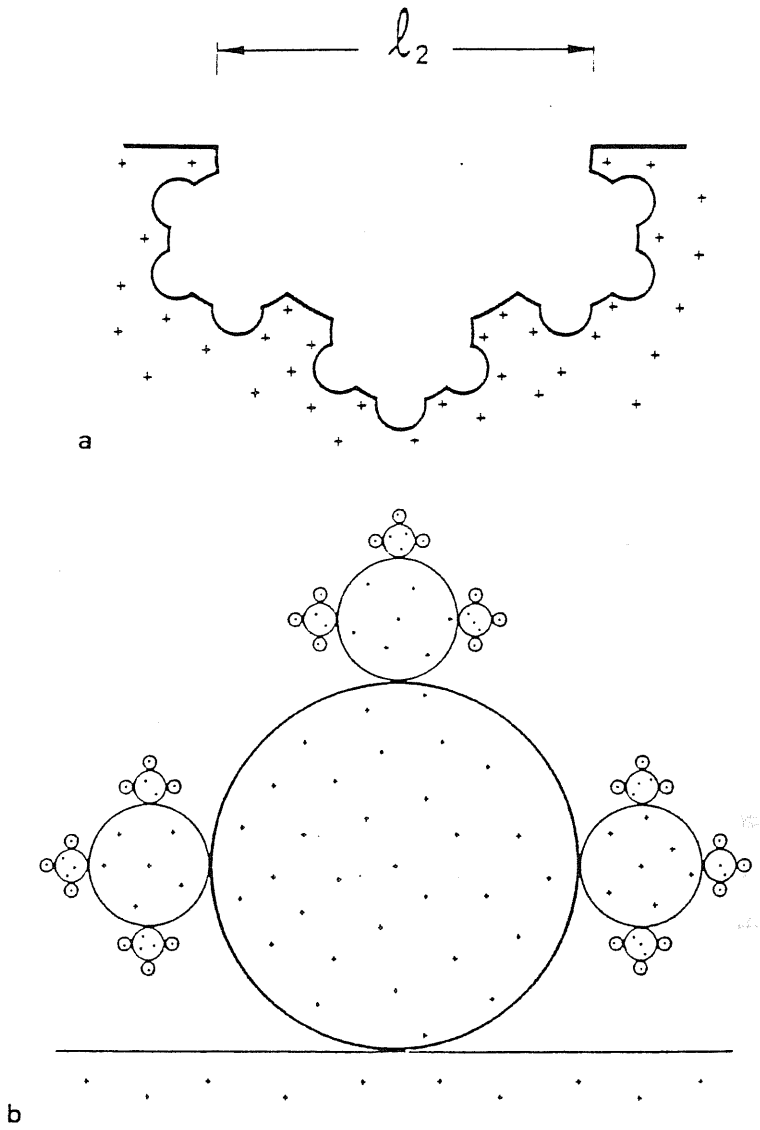

Fig. 2.7 The two models for fractal surfaces: *a*) iterative pits; *b*) iterative flocs.

$r(p)$. The problem of determining quantities like Ω is thus reduced to that of finding the correct $r(p)$ in the problem.

2.3.2 *MULTILAYER ADSORPTION ON A FRACTAL SURFACE*[10,39]

After the scaling argument of de Gennes, Pfeifer *et al.*[10] proposed a new phenomenological model for adsorption on fractal surfaces. The starting point of their approach is the Frenkel–Halsey–Hill (FHH) theory of adsorption on a

flat surface.[40–42] The adsorbate is treated as a continuum whose density and energy are only weakly perturbed by the substrate. In this theory the difference in chemical potential between a film of thickness z and the bulk liquid is given by the difference in the van der Waals dispersion energies, $\mu - \mu_0 = -\lambda z^{-3}$ (here λ takes into account both the adsorbate–substrate and adsorbate–adsorbate interactions, assuming the latter to be the same as in the bulk liquid). By equating the film (bulk) chemical potential to that of its coexisting vapor at pressure p (p_0), the film thickness z is given by the pressure–dependent length,

$$\zeta_p = \left[\frac{\lambda}{k_B T \ln(p_0/p)}\right]^{1/3} \tag{2.19}$$

To treat the non planar case, the authors imagine that at the interface between liquid film and vapor the principle of local thermodynamics is valid. This implies the equilibrium condition

$$\mu = \mu_{int}(\vec{r}) + v(\vec{r}) \tag{2.20}$$

where μ_{int} is the chemical potential of a uniform system at the local ($\vec{r}$ dependent) thermodynamic conditions and $v(\vec{r})$ is the external potential due to the substrate. Eq.(2.20) is valid if $v(\vec{r})$ is slowly varying, which is the case for sufficiently large distances from the surfaces. Neglecting surface tension effects and assuming small curvature for the equipotential (v) surfaces, the interface has to lie on an equipotential surface (these approximations lead to $\mu_{int} = \mu_0$). This leads to the result that the liquid condenses in those volumes where the potential v is less than or equal to $k_B T \ln(p/p_0)$.

With the assumption that the potential v depends only on the distance z from the surface and is given by $-\alpha z^{-3}$ as in the flat–surface case, the authors obtained that the film volume is $\Omega(\zeta_p)$ equal to the volume of the space points lying at a minimal distance $\leq z$ from the surface (see Fig.2.8) and ζ_p is given by eq.(2.19). From eq.(2.13) we have already seen that this quantity scales as $z^{3-\bar{d}}$. Thus the number of particles of size a in the film will scale as

$$N = \Omega(\zeta_p)/a^3 \propto a^{-\bar{d}} \left(\frac{\zeta_p}{a}\right)^{3-\bar{d}} \propto N_m \left(\frac{\zeta_p}{a}\right)^{3-\bar{d}} \tag{2.21}$$

where $N_m \propto a^{-\bar{d}}$ is the monolayer coverage for molecules of size a.[8] In spite of the similarity between eq. (2.21) and eq. (2.17), it is important to remark that

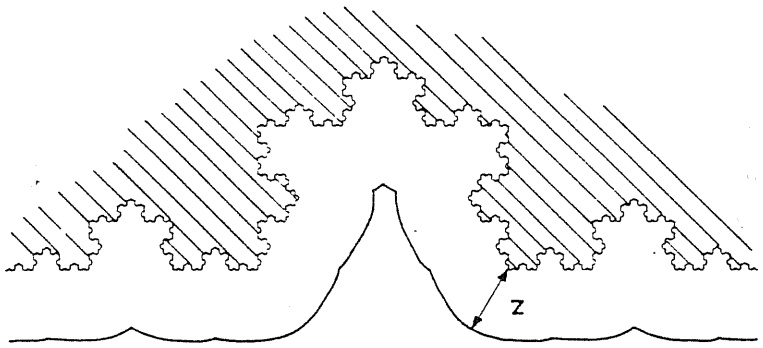

Fig. 2.8 Equipotential surface generated by a fractal substrate. It represents the film–vapor interface in the absence of surface tension. In the model, it consists of all points with the same (minimum) distance z from the substrate

this is only apparent. While in eq. (2.21) ζ_p represents the thickness of the wetting film, in eq. (2.17) r represents its curvature which in de Gennes'picture should have a precise dependence on the pressure p.

The authors have shown that eq. (2.21) holds also if the fractal surface is seen as a collection of pores, e.g., spherical pores (see Fig. 2.9), like in de Gennes' approach [9] (see previous section). The wetting of the surface is studied considering each pore as isolated and not connected to the others. Under these assumptions, a single pore is seen, e.g., as a spherical cavity of radius R in an infinite solid. Inside the pore cavity the potential energy v at distance z from the wall follow the expression [10]

$$v(z) = -8\alpha \left(\frac{R}{2Rz - z^2} \right)^3 \tag{2.22}$$

Within FHH theory, the film thickness z at pressure p (this means $k_B T \ln(p/p_0) = v(z)$), is given by

$$z(p,R) = \begin{cases} R - (R^2 - 2\zeta_p R)^{1/2}, & \zeta_p < R/2 \\ R(pore\ filling) & \zeta_p \geq R/2 \end{cases} \tag{2.23}$$

This equation reduces to the planar limit $z = \zeta_p$ when $\zeta_p \ll R$. To calculate the total film volume, the authors used the fact that the number of pores with radius between R and $R + dR$, for a fractal, scales as $R^{-\overline{d}-1}dR$. Thus the total volume of a film of thickness z' is

$$N \propto \int_0^{R_{max}} \omega(z', R) R^{-\overline{d}-1} dR, \tag{2.24}$$

where $\omega(z', R)$ is the volume of the layer in a pore of radius R with thickness z' ($\omega(z', R) = (4\pi/3)R^3$ if $R \leq z'$ and $\omega(z', R) = (4\pi/3)[R^3 - (R - z')^3]$ if $R > z'$). R_{max} is the upper cut–off of fractality. At pressure p, N is obtained by setting z' in eq. (2.24) equal to the equilibrium thickness of eq. (2.23)

$$N \propto \int_0^{R_{max}} \omega(z(p, R), R) R^{-\bar{d}-1} dR \tag{2.25}$$

The calculation of this integral gives for N an expression differing from that of eq. (2.21) only by a multiplicative constant, which is, on the other hand, of order unity.

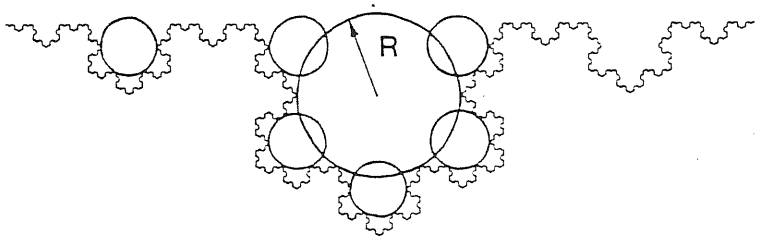

Fig. 2.9 Replacement of the fractal surface by a set of spherical pores of variable radius R

2.3.3 *SURFACE TENSION EFFECTS*[11]

Within the model discussed above, one can include in eq.(2.20) another term taking into account surface tension effects due to curvature. This equation becomes now [11]

$$v(\vec{r}) + 2\gamma/[\rho R_c(\vec{r})] = \Delta\mu \tag{2.26}$$

where $\Delta\mu = \mu - \mu_0$, γ is the liquid–vapor surface tension, R_c is the radius of curvature of the surface film at $\vec{r}$ and ρ is the density of the liquid. If the fractal surface is still considered as a collection of, e.g., spherical pores, eq. (2.26) has to be written for the points in the pore. With the potential (2.22) this equation becomes

$$-8\alpha \frac{R^3}{(2Rz_{loc} - z_{loc}^2)^3} - 2\frac{\gamma}{\rho(R - z_{loc})} = \Delta\mu \tag{2.27}$$

Here z_{loc} is the local thickness of the film inside the pore and $-(R - z_{loc})$ is the corresponding radius of curvature of its surface.(*) So, the total coverage over all the pores can be obtained similarly to eq. (2.24). Integration over the distribution of the pores gives

$$N \propto \int_0^{R_{max}} (4\pi/3)[R^3 - (R - z_{loc}(p,R))^3]R^{-\bar{d}-1}dR. \tag{2.28}$$

The quantity z_{loc} has to be evaluated for any value of R as a solution of eq.2.27. Looking at eq.(2.26) in the case of the interface of the liquid film of thickness r on a fractal surface, we see that at sufficiently high values of r the surface tension term will dominate. The assumptions that the first term scale as α/r^3 (as in previous section), and that the average radius of curvature of the interface at distance r from the interface is of the order r, led Pfeifer *et al.*[11] to an estimate of the critical thickness after which the surface tension term wins. This is given by

$$z_{crit} = \left(\frac{\alpha\rho}{\gamma}\right)^{1/2} \tag{2.29}$$

The numerical solution of eq. (2.27) and the integration of eq. (2.28) give for the total coverage the following limit scaling behaviours:

$$N \propto \begin{cases} \zeta_p^{3-\bar{d}} & \text{if } \zeta_p < z_{crit} \\ \zeta_p^{3(3-\bar{d})} & \text{if } \zeta_p > z_{crit} \end{cases} \tag{2.30}$$

Here ζ_p is always given by eq. (2.19).

2.4 ADSORPTION ON SELF–AFFINE SURFACES

Fractal surfaces are not the only possible model of rough surfaces. As already mentioned in sect. 2.2, also self–affine surfaces have been proposed to simulate rough substrates.[37] As remarked in ref. [10], when, e.g., the surface geometry is probed by scanning tunneling microscopy (STM), it is not possible to make a clear–cut distinction between fractal and self–affine surfaces.

(*) The radius of curvature is negative if the center of the tangent circle lies on the vapor side of the interface.

Self–affine surfaces, at variance with fractal surfaces, do not strictly display self–similar properties. The former ones can be described in terms of a single–valued function, $h_s(\mathbf{x})$, where $\mathbf{x}$ spans a $D = d - 1$ dimensional space. This kind of description is possible in connection with the fact that overhangs are irrelevant for self–affine surfaces. The roughness of a self–affine surface is characterized by the exponent ζ_s which controls the scaling behaviour of the mean height fluctuation across the length scale $|\mathbf{x}|$. One has

$$\langle |h_s(\mathbf{x}_0) - h_s(\mathbf{x}_0 + \mathbf{x})| \rangle \propto |\mathbf{x}|^{\zeta_s} \tag{2.31}$$

where the average $\langle \ldots \rangle$ is over all points $\mathbf{x}_0$ and, in the case of a random self–affine surface, also over different realizations of the surface.

Kardar and Indekeu[37] developed an interface approach for wetting on self–affine surfaces. In the limit of thick adsorbed layers, this approach lead the authors to write for the interface at a distance z from the substrate the following effective potential

$$U_e(z) = U(z) + CU''(z)\left(\frac{\gamma}{U''(z)}\right)^{\zeta_s}, \tag{2.32}$$

where U is the potential energy due to the interaction with the substrate, C is a constant and γ is the surface tension. $U(z)$ is essentially proportional to z times the substrate potential, $V(z)$, for a point at a distance z from the substrate. The second term of (2.32) represents the cost of deforming the interface by the substrate, because of surface tension.

Since long–range adsorbate–substrate interactions lead to a potential energy[43] $U(z) = u/z^{\sigma-1} + v/z^{\sigma} + \ldots$, (we usually assumed $\sigma = 3$, so far) the leading correction due to the surface tension, scales as

$$\delta U(z) \sim \gamma^{\zeta_s} u^{1-\zeta_s} z^{-(1-\zeta_s)(\sigma+1)} \tag{2.33}$$

The consistency requirement of a correction term weaker than the original potential, led Kardar and Indekeu to distinguish two cases as done also by Lipowsky and Fisher:[43] *a*) "*Mean field*" regime, $\zeta_s < \zeta^* = 2/(\sigma + 1)$, in which the asymptotic behaviour is dominated by the original potential $U(z)$. *b*) "*Strong–fluctuation*" regime, $\zeta_s > \zeta^*$, in which the surface tension cost dominates the original potential. In this second case the effective potential is obtained self–consistently from

$U_e(z) \sim \gamma^{\zeta_s} U_e''(z)^{1-\zeta_s}$ and gives

$$U_e(z) \propto \gamma / z^{2(1-\zeta_s)/\zeta_s} \tag{2.34}$$

In the case of complete wetting the thickness of the wetting layer is expected to diverge. To obtain the critical exponents, one has to include in the effective potential of eq. (2.33) also the thermal fluctuations effects. This gives rise, in the linearized scheme of Kardar and Indekeu, to a further term in (2.33) of the type $c'(U''(z)/\gamma)^{1-\zeta_0}$, $\zeta_0 = 1 - D/2$ being the roughness exponent of a free interface.[43] So, the predominance of a $U(z)$ or of a surface tension character in the asymptotic behaviour of $U_e(z)$ is determined by the larger of the two exponents ζ_s and ζ_0.

The amount of adsorbed material on the surface is obtained by evaluating the volume of the space between the substrate and the interface. For a thickness z of the adsorbed layer, this volume is proportional to the coverage $N(z)$ which satisfies the following equation

$$N(z) = Az + Bz^{\phi} \tag{2.35}$$

Here A and B are constants. The above results for the scaling of the correction term of the effective potential give[37] $\phi = \zeta_s(\sigma+1) - \sigma$ in the "mean field" regime, while $\phi = (3\zeta - 2)/\zeta$ in the "strong–fluctuation" regime, with $\zeta = \max(\zeta_0, \zeta_s)$.

Eq. (2.35) shows that in a self–affine substrate, asymptotically, $N(z) \propto z$. However, z diverges as $(\mu_0 - \mu)^{-\psi}$. The Kardar and Indekeu scheme give the following results: in the case of van der Waals interactions (e.g., $\sigma = 3$ as previously assumed) $\psi = 1/3$ in the "mean field" case, and $\psi = \zeta_s/(2 - \zeta_s)$ in the "strong–fluctuation" regime.

2.5 CONCLUDING REMARKS

In this chapter we have reported some of the theoretical approaches to adsorption and wetting on self–similar and self–affine surfaces. The picture which can be extracted from the results of these approaches is somewhat confusing.

The similarity of the coverage scaling behaviours given by schemes in sects. 2.3.1 and 2.3.2 or 2.3.3 is only apparent. While in eqs. (2.17) and (2.18) the main

variable is the radius of curvature of the interface of the adsorbed film, in eqs. (2.21) and (2.30) ζ_p represents the thickness of the adsorbed layer. It should be stressed that in the above schemes the connection between these two quantities is not clear. Moreover, it is at least somewhat ambiguous the meaning of the adsorbed layer thickness mentioned in 2.3.3, because in the presence of pore–filling effects no clear definition of layer thickness is possible, as we will see in the next chapter.

The ambiguities and drastic approximations of the above approaches, convinced us that more microscopically minded and realistic modellizations should be considered in order to get a clear picture of adsorption and wetting phenomena on rough substrates. A model which could hopefully open new perspectives in this direction is discussed in the next chapter.

CHAPTER 3

A LATTICE–GAS MODEL FOR WETTING ON SELF–SIMILAR SURFACES

Wetting in the presence of rough substrates is of particular interest because, as indicated by the simplified model considerations and scaling arguments of the previous chapter, its study could give information on the geometrical properties of the surfaces. In addition to this, the thermodynamic aspects of the adsorption process on rough substrates are worth studying in themselves. However, in spite of the many phenomenological approaches proposed in the literature, we are still far from a satisfactory understanding of this issue.

The survey we presented in Chapter 2 should already have suggested us that wetting on rough substrates needs more detailed modellizations. Satisfactory models should be able both to take into proper account the geometrical scaling properties of the surfaces, and to include all the ingredients for a correct physical description of wetting.

3.1 A LATTICE–GAS MODEL FOR ADSORPTION ON A FRACTAL SUBSTRATE[44]

In this section we present results of extensive calculations performed on a lattice–gas model for adsorption on a deterministic fractal surface. The advantages with respect to previous approaches are many. The model embodies a real

fractal surface, which is described in its full complexity, without resorting to approximations like that of treating it as a collection of independent pores, with power–law distributed sizes.[10,9,11] The lattice–gas description takes into account microscopically the effects of both adsorbate–substrate and adsorbate–adsorbate interactions. Futhermore, the statistical mechanical treatment allows a discussion of the effects of temperature and a full characterization of the thermodynamics of adsorption isotherms.

3.1.1 *THE MODEL*

The model, as mentioned above, is based on a lattice–gas description. The calculations are performed in the mean field (MF) approximation. In a certain way, the model generalizes previous theoretical investigations of adsorption on flat surfaces.[21,22] The generalization we have accomplished here is highly non–trivial. To obtain a sensible description of a system in which one has no more translational, but scale invariance, one has to include self–similarity over many length scales. Because of these facts, one can easily see that the number of distinct order parameters to be handled for a sensible calculation increases enormously. In view with these complications and in order to reduce computational problems, we worked with a two–dimensional system.

The system is constituted by a finite box in square lattice (Fig. 3.1). A contour (heavy line) marks the separation between the solid substrate and the region accessible to the adsorbed fluid. All lattice sites belonging to the lower part of the lattice, including the contour, are occupied by centers of atoms of the solid substrate (crosses). The remaining sites (heavy and light dots) are accessible to gas molecules.

Now, the lattice–gas model can be build–up in the following way: to each site i of the upper part of the lattice we associate the occupation number $n_i = 0, 1$ that correspond to the presence, or the absence, of a gas molecule respectively. Hard–core repulsions between molecules are thus taken into account as usual in a lattice–gas description. On the other hand, long–range attractive interactions have to be explicitly included in the Hamiltonian that will assume the following

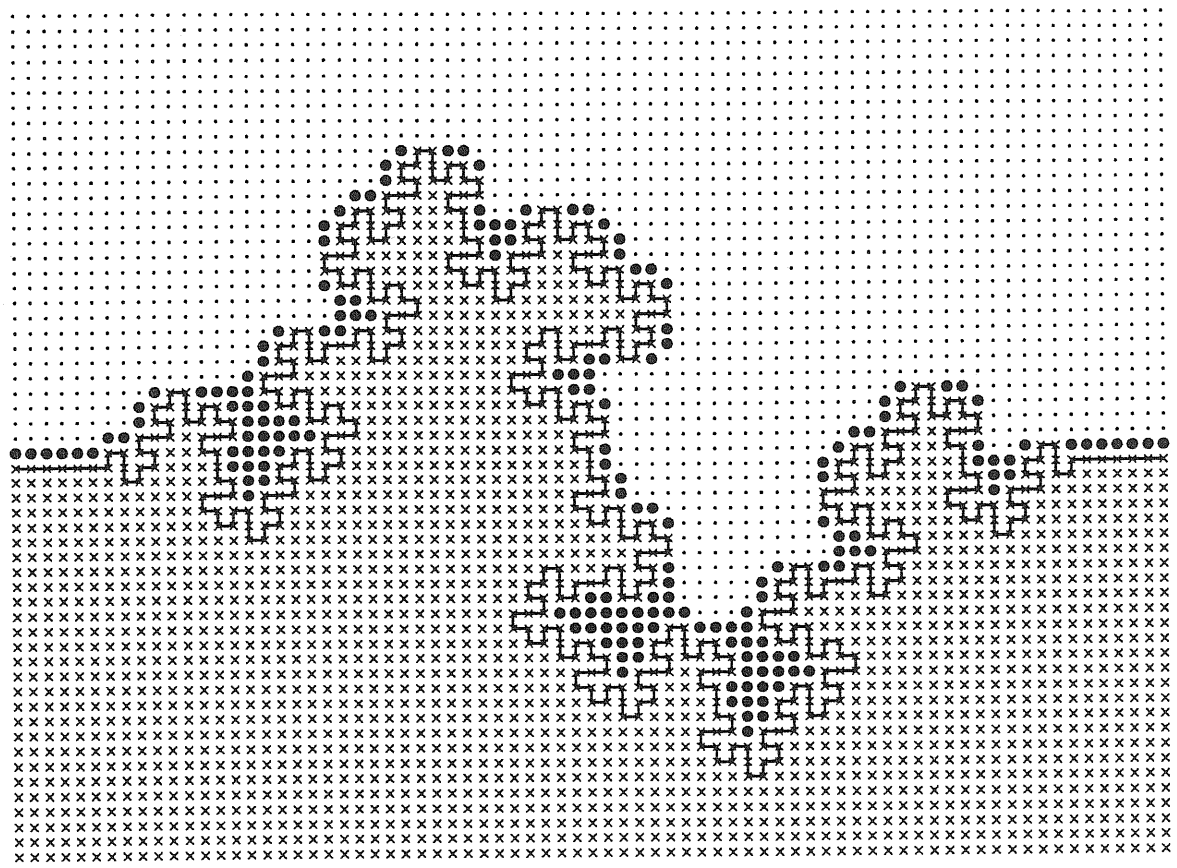

Fig. 3.1 Sketch of the box used in the calculations. Heavy dots, on sites with $\rho_i \geq 0.8$, represent the molecules of adsorbed gas constituting the film in a particular solution of eq.(3.6).

form:

$$\mathcal{H} = \sum_i V_{Si} n_i + \frac{1}{2} \sum_{i,j} V_{ij} n_i n_j \tag{3.1}$$

where the sums are over the sites not belonging to the solid and

$$V_{Si} = -\alpha \sum_{j \in solid} 1/|\mathbf{r}_j - \mathbf{r}_i|^6 \tag{3.2}$$

is the potential at site i, given by the attractive ($\alpha > 0$) van der Waals interactions with the solid atoms, and V_{ij} is a nearest neighbor (n.n.) attractive potential: $V_{ij} = -\varepsilon$ if i and j are n.n., $V_{ij} = 0$ otherwise. In eq.(3.2) and in all this chapter we consider the vectors $\mathbf{r}_i$ and $\mathbf{r}_j$ and the distances measured in units of the lattice spacing, a. Therefore the parameter α actually represents the van der

Waals interaction energy between a gas molecule and a solid atom a distance a apart.

As seen in Fig. 3.1, our contour has the feature of being fractal (, the fractal dimension of the contour is $\overline{d} = 3/2$ in our example), i.e., self similar,[1] on a range of scales between the lattice spacing and an upper cut–off (64 lattice spacings in Fig. 3.1). A sketch of the fractal contour used in our model is reported in Fig. 1.2 Because of the self–similarity of the contour the potential V_S has to be calculated numerically as just written in eq. (3.2), without the possibility of resorting to some analytical approximation.

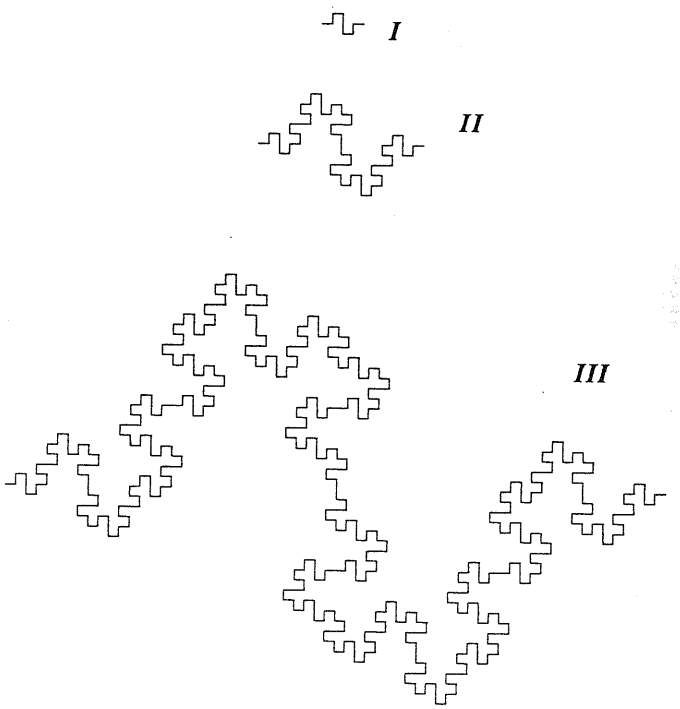

Fig. 3.2 The fractal contour used in our model. The curve is obtained by making use of the construction scheme sketched in the figure. I, II and III are the first three steps of the construction. From this scheme it is clear that the fractal dimension of the curve is $\overline{d}$=ln 8/ln4=1.5.

The two–dimensional character of the system is not a crucial limitation, since our model should have mostly a qualitative value. On the other hand, one can also look at it as at one describing peculiar situations in the real, three–dimensional

world. Indeed, Fig. 3.1 can be seen as the transversal section of a real surface, having translational invariance in direction perpendicular to the figure, and fractal dimension $\overline{d}+1=2.5$. Of course, potentials like V_{Si}, should be reinterpreted, in this case, as representing the interaction of a given gas molecule with a full row of atoms in the solid. A $1/r^6$ molecule–row potential, e.g., would result from a $1/r^7$ molecule–atom interaction. Also V_{ij} should be modified consistently.

Let us now describe the system in the grand canonical ensemble. The pressure p of the gas is replaced by the chemical potential μ. It is well known that treating the vapor as an ideal gas, pressure p and μ are related by the following relation

$$p/p_0 = \exp((\mu-\mu_0)/k_BT) \tag{3.3}$$

where p_0 and μ_0 are pressure and chemical potential at coexistence, respectively. In the MF approximation the occupation numbers n_i are replaced by their average values $\rho_i=\overline{n}_i$. The free energy of the system is given by the minimal value of

$$\mathcal{F}=k_BT\sum_i[\rho_i\ln\rho_i+(1-\rho_i)\ln(1-\rho_i)]+\sum_i(V_i^S-\mu)\rho_i+\frac{1}{2}\sum_{ij}V_{ij}\rho_i\rho_j \tag{3.4}$$

for given μ and T.

The extremalization of $\mathcal{F}$ can be obtained by imposing the following set of conditions

$$\frac{\partial\mathcal{F}}{\partial\rho_k}\equiv 0 \tag{3.5}$$

which can be written as:

$$\rho_k=\frac{1}{1+\exp\left[(V_k^S+\sum_j V_{kj}\rho_j-\mu)/k_BT\right]} \tag{3.6}$$

Since we are obliged to use a finite box (Fig. 3.1), we choose the flat lateral portions of the boundary sufficiently long (see below), and the boundary conditions on the vertical sides of the box periodic. In this way we approximate very well the situation of a finite fractal boundary interrupting an infinite flat one. The upper side of the box is chosen far enough from the tips of the fractal boundary. On this side we impose

$$\rho_i=\rho_\infty=\frac{1}{1+\exp\left[(\rho_\infty\sum_k V_{ik}-\mu)/k_BT\right]} \tag{3.7}$$

where ρ_∞ is the density of the bulk vapor phase.

3.1.2 *STRATEGY FOLLOWED IN THE CALCULATIONS*

Most of our calculations were performed on a 104×102 box, with an upper cut–off for fractality of 64 lattice units. Other results were obtained on a 336×272 box, with cut–off 256. Of course in the latter case it is possible to test substantially higher coverages before experiencing a cross–over from fractal to flat adsorption.

Because of the fact that V_S has to be calculated numerically, some cares has been considered. For any site of the lattice available to the gas molecules, V_S has been evaluated including in sum (3.2) all the solid atoms at a distance from the site large enough to have a relative error in V_S smaller than 0.5%. The error was evaluated by comparing the V_S obtained for distances of solid atoms up to a certain, e.g., R^{max}, with that in the case in which for distances larger than R^{max} the substrate is replaced by an infinite lattice. Both the width of lateral parts of the boundary, and the cut–off in the sum (3.2) were always chosen in such a way to guarantee an accurate evaluation of V_S in all the region occupied by the adsorbed film. Most of the calculations of the present work were performed on a CRAY Y–MP 432.

One of the most important quantities to which one is interested studying wetting is the coverage, that is the amount of material adsorbed on the surface. To evaluate this quantity, in our case, we have to calculate the excess density of the gas in the vicinity of the substrate. Following what reported in Chapter 2 (see eq.(1.1)), we defined the following coverage parameter:

$$\theta = \frac{1}{N_m} \sum_i (\rho_i - \rho_\infty) \tag{3.8}$$

where the sites over the lateral flat boundaries are not included in the sum, and N_m represents the number of sites building up a geometrical monolayer on the fractal portion of the boundary. These are the sites at unit minimal distance from the boundary itself. The normalization is of course not strictly necessary, and only chosen for convenience.

Solutions of (3.6) have to be found by numerical iteration. A non–trivial problem consists in singling out the solution which correspond to an absolute

minimum of (3.4), at given T and μ. Indeed, especially at low T, it turns out that the free energy can have many unstable minima, which can be reached with different initial ρ_i's in the iterations. The fractal nature of our boundary can be expected to cause a rich structure of minima; this structure reflects the strong hysteresis effects found, e.g., in the wetting of real porous materials.[27]

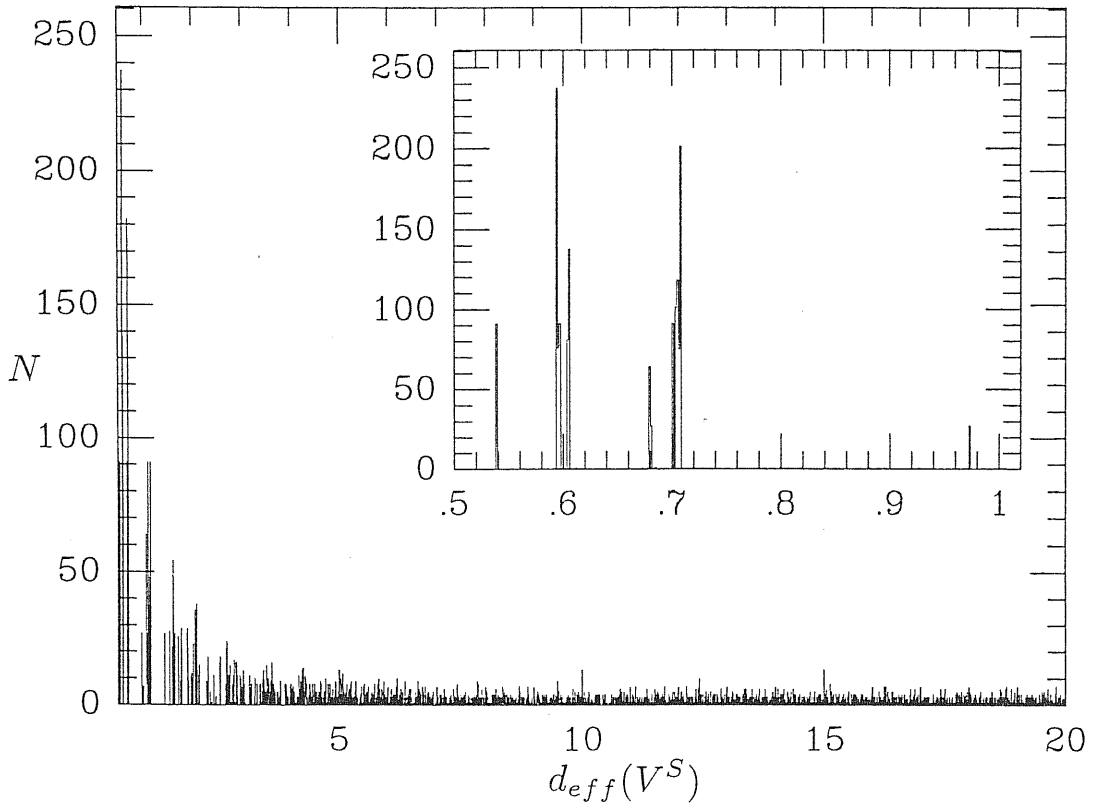

Fig. 3.3 Hystogram of the number of lattice sites as a function of $d_{eff}(V_S)$.

We performed an exploration of the minima structure by trying, at each (T, μ), a considerable number (up to thousands) of randomly chosen initial conditions. The procedure, combined with suitable variations of the temperature during iteration, turned out to be reasonably efficient for our purposes.

3.1.3 *THE SUBSTRATE POTENTIAL AND THE NATURE OF THE ISOTHERMS*

For planar substrates it is well known[21] that the isotherms, at low T and not to high ε/α, present almost flat plateaus at coverages $\theta = 1, 2, 3 \ldots$ (see also Chapter 2). The regions between subsequent plateaus are characterized by a faster and generally discontinuous increase of θ as a function of μ. The discontinuities associated to the vertical steps in the isotherms amount to first order transitions, each one corresponding to addition of an extra layer to the adsorbed film.

Whether in the fractal case such kind of plateaus and transitions should be expected, or not, is far from clear, a priori. Iso–V_S curves are not uniformly spaced and closed curves also occur.[45] The non–uniform spacing implies that, if we plot on a hystogram the number of lattice sites as a function of $d_{eff}(V_S) = \left(\frac{3\pi}{32}|\alpha/V_S|\right)^{1/4}$, the situation is very different from that of a flat substrate.(*) In the latter case the plot consists of a sequence of equally spaced, δ–like and equal strength peaks, each one located at the d_{eff} value corresponding to the thickness of a given layer of adsorbed molecules. On the other hand, for our fractal surface, if the range of the adsorbate–substrate interactions is infinite, δ–like distributions of points in the hystogram can not occur, strictly. However, at reasonably low d_{eff}, there are still some peaks (Fig. 3.3), as a consequence of the fact that thermodynamically significant fractions of the points accessible to the adsorbate turn out to have very close values of V_S. For higher values of d_{eff} the situation rapidly changes: both the strength of peaks, and the spacing between them becomes smaller and smaller.

It has been proposed that the distribution of sites should decrease to zero for increasing d_{eff} as $d_{eff}^{-(2-\bar{d})}$.[45] This is essentially based on the fact that in spite of the fractality of the surface, the bulk substrate constitutes a three–dimensional object (two–dimensional in our case). So, because of the fact that for a three–dimensional substrate the potential scales with the distance as $V \propto 1/r^3$, and the number of sites in the vicinity of fractal substrate having a potential $\leq V$ scale as $r^{3-\bar{d}}$ (see also eq. (2.1)), one sees that the mentioned behaviour is obtained (;the

(*) $d_{eff}(V_S)$ can be seen as an effective distance from the fractal boundary, suggested by the fact that, in the flat case, $V_S \simeq -\frac{3\pi}{32}\alpha/d^4$, for a point at distance d.

distribution is proportional to the derivative of the quantity we obtained here). In the range of distances tested by our calculations the convergence of the potential V_S to a $1/r^4$ (, the exponent 4 instead 3 is due to the two–dimensional character of our system,) is not very fast. We found that for a range of distances of about 10 lattice spacing V_S a power law is not followed strictly.

For a flat substrate, each first order transition, corresponding to addition of an extra layer of molecules, is determined by the combined effect of the adsorbate–adsorbate interaction, and of the occurrence of a δ–like peak in the above hystogram. Since in the fractal case we can still identify a few, relatively sharp peaks at rather low d_{eff}, we can expect to find, in correspondence to them, transitions governed by mechanisms similar to those of the flat case. On the other hand, transitions corresponding to inclusion in the layer of sites not contributing to the peaks, must be governed by different mechanisms. It should also be remarked that, since the fractal has non–zero curvatures, surface tension effects should influence film formation and coverage transitions.

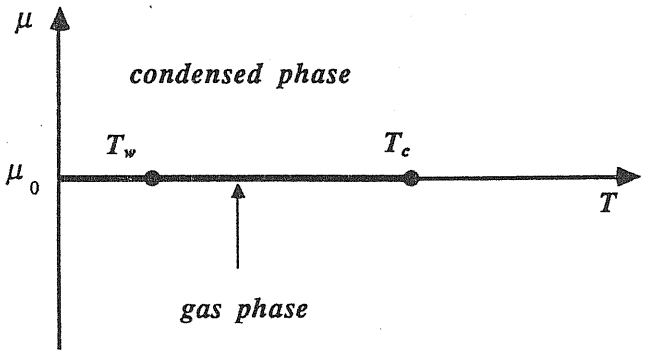

Fig. 3.4 Schematic phase diagram of our system. T_c is the critical temperature. The arrow in the gas phase region indicates the path one has to follow to get an isotherm in our model. If $T>T_w$, the wetting temperature, the path leads to observation of the phenomenon of complete wetting, upon approaching the T axes. In the cases considered here $T_w=0$.

3.1.4 *THE ADSORPTION ISOTHERMS: LOW COVERAGE REGIME*

Most of the informations on wetting of a surface can be obtained by the

analysis of adsorption isotherms. In fact, these isotherms are also relatively easy to be recorded by experimental techniques as already reported in Chapter 1.

In a real system, to deal with adsorption isotherms means to approach the sublimation curve (i.e. solid–gas coexistence line) from the gas phase region (see Figs. 2.3(a) and 2.3(c)). On the contrary, approaching again from the gas phase region the liquid–gas coexistence line one has the opportunity to monitor the known wetting phenomena as pre–wetting, critical wetting and complete wetting described in Chapter 2. In our model there is not the possibility to have all the three phases one finds in nature. From eq.(3.7) one could see that for the bulk only two phases can be distinguished. At temperatures lower than T_c (for our model $T_c = \varepsilon/k_B$, in the MF approximation) one observes a first order transition between them. We will call these two phases: gas phase and vapor phase respectively. This situation is summarized in Fig.3.4 where a schematic phase diagram for our system is reported.

We report here isotherms in the low coverage range for two different values of both T and ε in Figs. 3.3a, b. Here we chose as natural variable $d_{eff}(\Delta\mu) = \left(\frac{3\pi}{32}|\alpha/\Delta\mu|\right)^{1/4}$ with $\Delta\mu = \mu - \mu_0$. This d_{eff} is the thickness of a layer growing at $T = 0$, and $\varepsilon << \alpha$, on a flat substrate. From Figs. 3.5a, b, It is clear that first order transitions take place in all cases. It can also be seen that a few of them are in correspondence with the peaks of Fig. 3.3. A strict coincidence of the values of d_{eff} in the two figures could only occur for very low ε/α and T. Anyway, the correspondence is restricted to a very low d_{eff} range, becoming even narrower as ε is increased. From this fact, we can conclude that these transitions are essentially controlled by V_S in much the same way as in the case of flat substrate. On the other hand, the transitions occurring at higher $d_{eff}(\Delta\mu)$ do not correspond to peaks of Fig. 3.3. We conclude in this case that they are primarily determined by surface tension effects. At variance with the flat case, it is remarkable that plateaus occur at generally non–integer θ's and θ–jumps at the transitions are not close to integers. Moreover, variations of ε turn out to affect sensibly the structure of the isotherms. This fact is clearly due to surface tension effects becoming increasingly important at higher values of ε.

There were claims, recently, that performing adsorption measurements, e.g.,

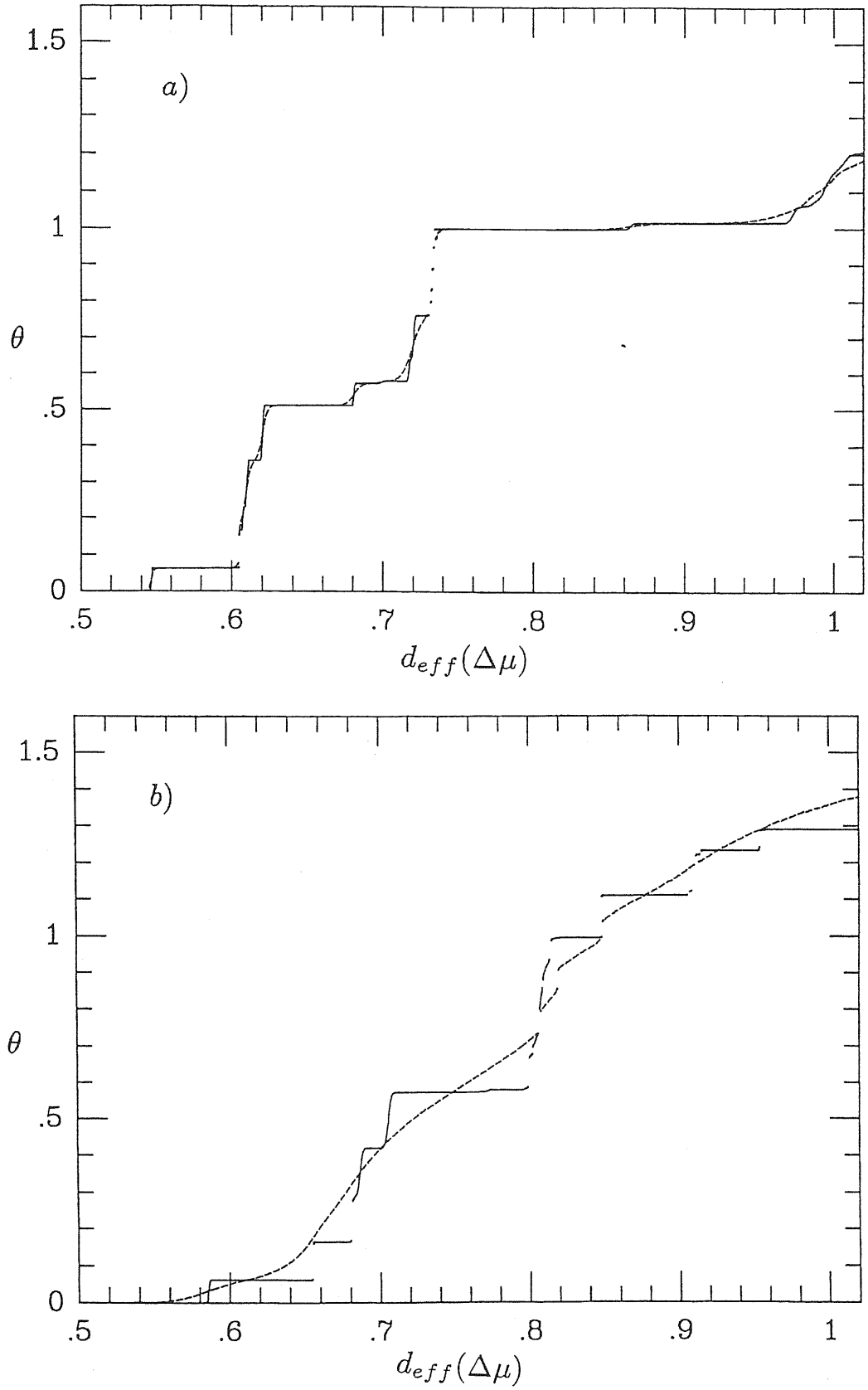

Fig. 3.5 Example of isotherms for the low coverage regime: *a*) corresponds to ε/α=0.1 (full line $k_B T/\varepsilon$=0.02, dashed line $k_B T/\varepsilon$=0.2), while in *b*) ε/α=0.5 (full line $k_B T/\varepsilon$=0.01, dashed line $k_B T/\varepsilon$=0.4). Major interruptions of the lines mark first order discontinuities.

with two different kinds of molecules, of linear sizes a and a', respectively, should lead to a very simple result for $\overline{d}$.[8] Indeed, if one is guaranteed that proper (i.e., geometrical) monolayer adsorption ($\theta = 1$) occurs and can be detected in both cases, one expects

$$\frac{\overline{N}'_m}{\overline{N}_m} = \left(\frac{a}{a'}\right)^{\overline{d}} \quad (3.9)$$

with $\overline{N}_m$ and $\overline{N}'_m$ representing the measured numbers of molecules forming the monolayers in the two cases. The isotherms we report in Figs.3.3a, b seem to put some shadow on this possibility. If we take into account our model plateaus are present for fractional and strongly ε–dependent values of θ and then the application of eq.(3.9) becomes quite ambiguous. Already with very small ε, plateaus occur also at non–integer θ. Even the occurrence of $\theta \simeq 1$ in our model corresponds to the formation of "monolayers", which are in fact disconnected and have nothing in common with a geometrical monolayer.

An example of this fact is shown in Fig. 3.6. Here we can see how for two different values of the ratio ε/α in spite of the close values of θ the shape of the film can be significantly different. As displayed in Fig. 3.6 this phenomenon have important consequences not only in the high coverage regime, but also in the very low coverage regime. The occurrence of such phenomenon, due, of course, to surface tension effects, suggest us that the concept of monolayer in such a system is not so clearly defined. This should be carefully taken into account in the evaluation of monolayer coverage from experimental data.

3.1.5 *THE PHASE DIAGRAM*

Fig. 3.7 gives the (θ,T) phase diagram for ε and α equal to the values taken in the case of Fig. 3.5b. Each bell–shaped curve in this figure, points at the same temperature correspond to the θ–values of coexisting phases. The μ values at coexistence turned out to be almost independent of T for each coexistence curve. Only in one case (see arrow in Fig. 3.7) we could detect a sensible dependence of the coexistence μ on T.

The phase diagram shows a rather complex structure. This also reflects the fact that two different transition mechanisms coexist in this low–coverage range, as

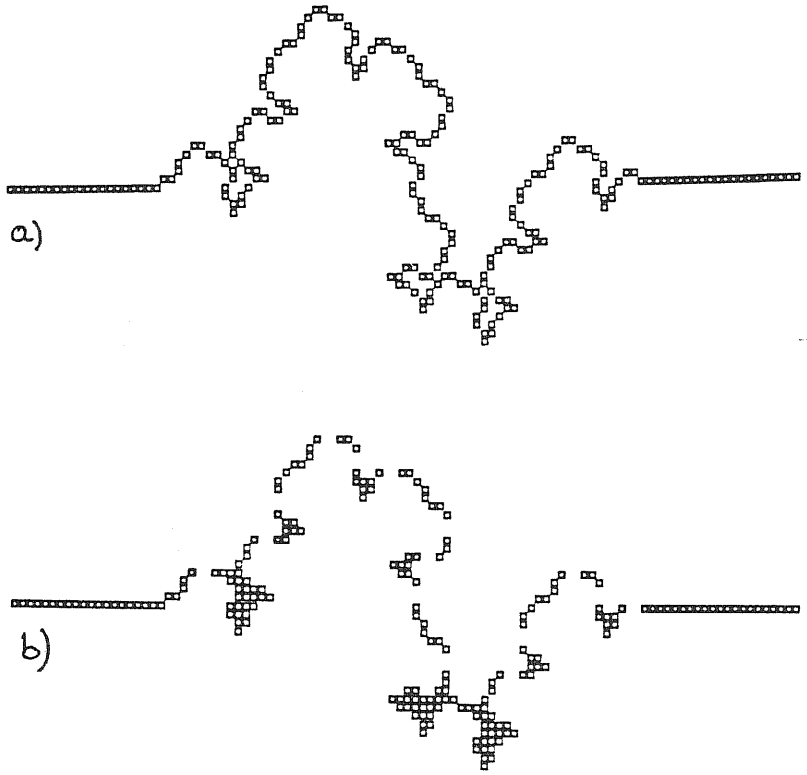

Fig. 3.6 Two examples of adsorbed films with $\theta \simeq 1$ relative to two different values of the ratio ε/α. The small squares represent the sites where $\rho_i \geq 0.8$. Both the films were obtained setting $d_{eff}=0.82$, while in *a*) $\varepsilon/\alpha=0.1$ and in *b*) $\varepsilon/\alpha=0.5$.

discussed above. Within the accuracy of the numerical exploration, all first order discontinuities, except one, turn out to go to zero at critical temperatures for which the transitions become second order. The relatively limited range of θ considered, and the rather irregular appearance of the coexistence regions do not allow any speculation concerning possible general trends, e.g., for the critical temperatures, $T_{c,n}$, as a function of coverage. Like in the case of a planar substrate,[21,22,46] it would be very interesting to address this problem, and we plan to do it in a future publication.[47]

3.1.6 *ISOTHERMS IN THE MULTILAYER REGIME*

The multilayer adsorption regime ($\theta > 1$) is also one from which one hopes to extract information on $\overline{d}$ for a fractal surface. Pfeifer and coworkers[10] (see also

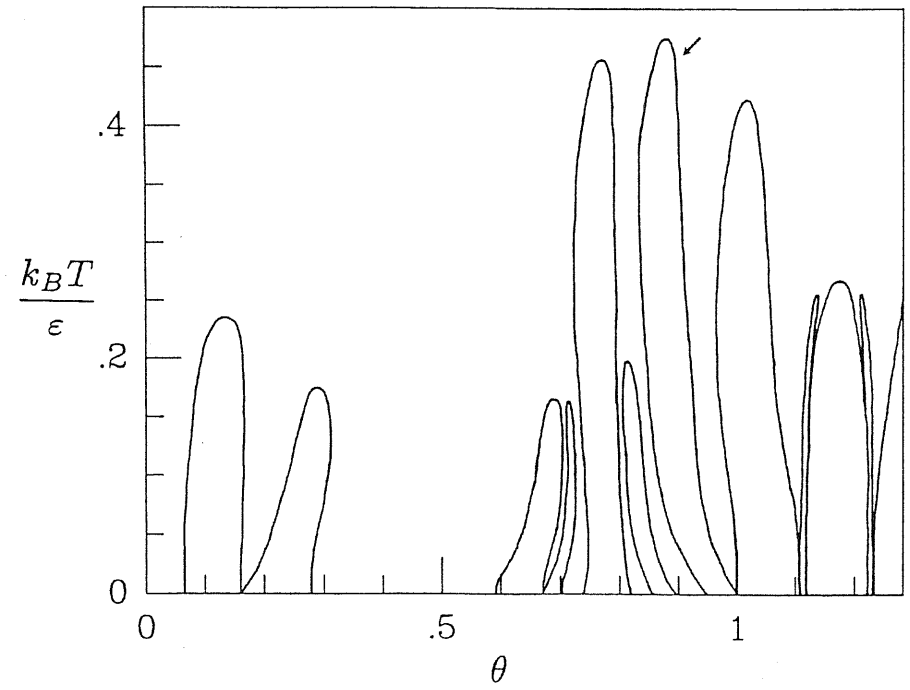

Fig. 3.7 Low coverage (θ,T) phase diagram for ε and α fixed at the values taken in Fig. 3.5*b*.

sect. 2.3.2) addressed this problem, predicting a power law of the form

$$\theta \underset{\Delta\mu\to 0^-}{\sim} |\Delta\mu|^{-(3-\bar{d})/3} \tag{3.10}$$

The idea at the basis of this result is to consider the fractal as a collection of independent, e.g., spherical, pores, distributed in such a way that $dn \sim R^{-\bar{d}-1}dR$ gives the number of pores with size R in the range $R \vdash\dashv R + dR$. A slightly different model based on similar ideas were proposed also by de Gennes [9]. On the basis, of a refined version of this model in which also surface tension were taken into account, Pfeifer *et al.* [11] pointed out the possibility of a cross–over from the behaviour (3.10), essentially determined by V_S, to the new one:

$$\theta \underset{\Delta\mu\to 0^-}{\sim} |\Delta\mu|^{-(3-\bar{d})} \tag{3.11}$$

for $\Delta\mu$ greater than some $\Delta\mu_c$. In the asymptotic regime (3.11) surface tension dominates with respect to V_S. At $\Delta\mu \simeq \Delta\mu_c$ the "thickness" of the multilayer

can be expected [45,37] to be in the range $10 \div 20\mathring{A}$ in the situations considered in recent experiments [10] While experimental evidence, up to now, seems to support, to some extent, the behaviour (3.10), no clear signals of a cross–over to (3.11) could be perceived from the results.

Recently this also led other authors to question the validity of a fractal assumption for the substrates examined, and to propose an alternative explanation in terms of self–affinity. [37,48] These authors indeed assumed self–affinity for the rough surfaces of the samples in ref. [10]. By then applying the results of their approach, reported in sect. 2.4, they concluded that the data could be interpreted on the basis of this assumption with a ζ_s exponent equal to $\simeq 0.37$, implying a "strong fluctuation" regime.

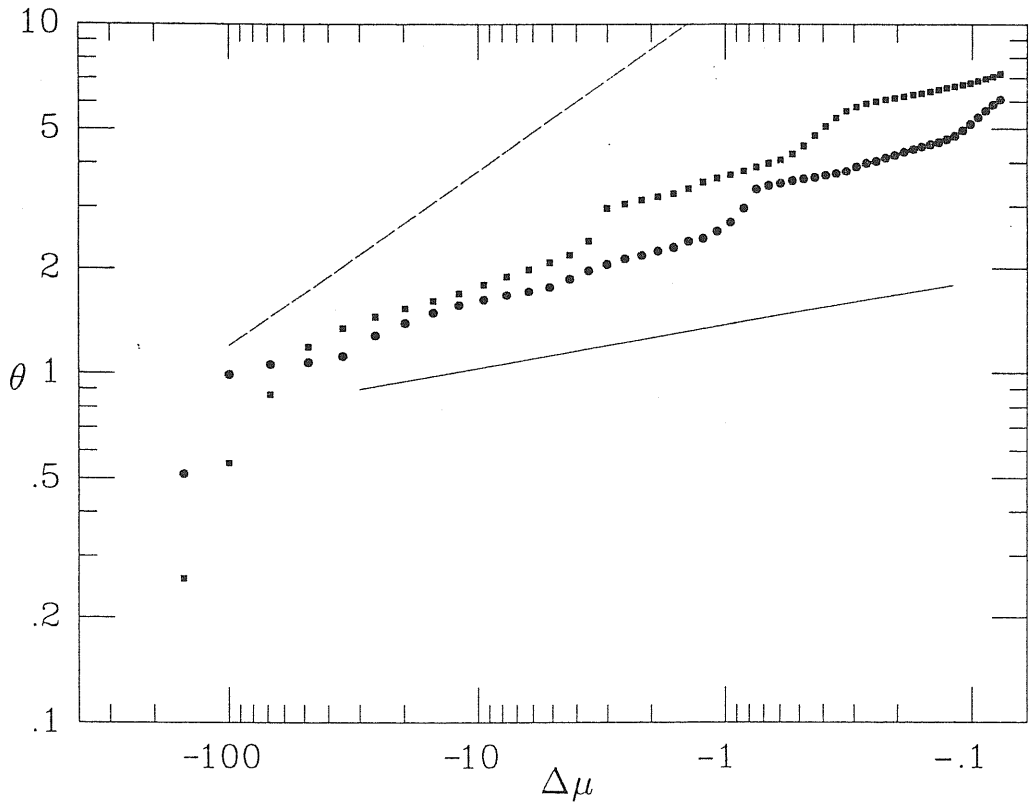

Fig. 3.8 High coverage (θ>1) isotherms for ε/α=0.1 and $k_B T/\varepsilon$=0.4 (circles), and ε/α=0.5 and $k_B T/\varepsilon$=0.6 (squares). The full and dashed lines represent the slopes corresponding to eqs. (3.10) and (3.11), respectively. These results were obtained with a 336×272 box size.

Our model allows to get insight into this controversial issue. We performed extensive calculations of θ as a function of $\Delta\mu$, at α and T fixed, with two different values of ε. The results are reported in the log–log plot of Fig. 3.8.

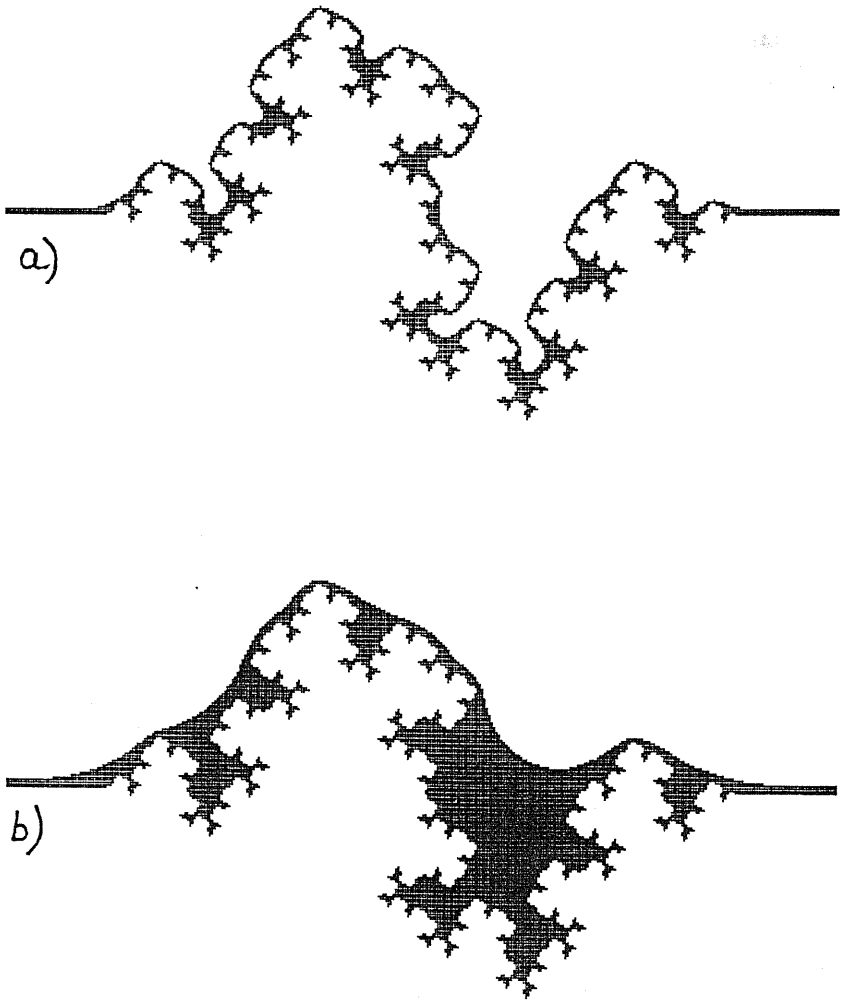

Fig. 3.9 Examples of adsorbed films in the high coverage regime. Here $\varepsilon/alpha$=0.5 and $k_B T/\varepsilon$=0.6. *a*) correspond to $\Delta\mu/\varepsilon$=−0.06 while in *b*)$\Delta\mu/\varepsilon$= −0.002. As previously the squares in the figure represent the sites where $\rho_i \geq 0.8$.

Due to the two–dimensional character of our model, the exponents in eqs. (3.10) and (3.11) should become $-(2-\overline{d})/4$ and $-(2-\overline{d})$, respectively. The results clearly show that it is very hard, if not impossible, to recognize in the plots shapes even roughly consistent with either one of these exponents. Surface tension

has the important effect to cause rather sudden coverage jumps in correspondence to the filling of pores of the surface. These jumps seem to replace, somehow, a definite cross–over to a new power law dependence, which is not observed in the explored range. In a model with continuously distributed pores one can not obtain such jumps. On the other hand, we believe that the presence of discrete typical pore sizes, as realized in our case, should be seen as a rather realistic feature.[27]

From Fig. 3.8 one can see that the jumps do not constitute single discontinuities in the isotherms. A more careful analysis show that they are characterized by a fine structure of smaller jumps corresponding to intermediate values of the coverage. This phenomenon is consistent with the fact that, in spite of the occurrence of pore filling, the lattice nature of the model determine a competition with the natural layering process typical of lattice models.

It should be noticed that, due to the rapid pore fillings on the surface, one reaches quite soon ($\theta \simeq 8$) film shapes, beyond which it is not legitimate anymore to disregard finite size effects.

In Fig. 3.9 are reported two examples of adsorbed films in the high coverage regime. From the figure one see clearly that because of the surface tension effects there is no more the possibility of define a specific thickness for the films, in particular as much as $\Delta\mu$ approaches zero. On the other hand, it has to be noted the marked effects caused to dewetting phenomena in the vicinity of the tips of the fractal surfaces. This fact determine that also at high coverage the thickness of the film in the tips remain small.

3.2 CONCLUSIONS

Summarizing, we presented here the first statistical model calculation of gas adsorption on a fractal surface. Besides showing a very rich and unsuspected structure for the adsorption isotherms, the results clearly indicate that both monolayer adsorption with different gases, and multilayer adsorption, are not very suitable for determining $\overline{d}$. Fractality in a proper geometrical sense, combined with adsorbate–adsorbate interactions leads to behaviours which do not seem fully consistent with the results of the schematic models and simple scaling arguments reported in

In the case of monolayer adsorption ideas for the determination of $\bar{d}$, we can say that the assumptions on which they are based are not easily verified in most real situations. A necessary condition for assuring the validity of the proposals of ref. [8] is that the adsorbate–substrate interactions are really much stronger than the adsorbate–adsorbate ones. Another possibility for the geometrical monolayer picture to be still meaningful, is perhaps given when the fractal dimension of the surface turns out to be very close to 2.

As to multilayer adsorption and wetting, we believe that the cross–over to the asymptotic regime of eq. (3.11) should be finally observed in a calculation producing more asymptotic coverages. The steep rises which can be observed in the isotherms of Fig. 3.8 are due, as already mentioned, to pore–filling effects and thus to surface tension. On the basis of model considerations of the type of those developed in sect. 2.3, we can expect that the isotherms in our model should asymptotically acquire a sort of staircase structure, each stair corresponding to the filling of a class of pores. The staircase character is due to the fact that our model surface contains only pores whose sizes are discrete multiples of a given elementary size $(a, 4a, 4^2a, \ldots, 4^n a, \ldots)$. At the same time, the number of the pores of size $4^n a$ is proportional to $(4^n a)^{-\bar{d}}$. One can thus see that such staircase should be asymptotically made of equal horizontal and equal vertical steps in the scales of Fig. 3.8. The resulting average slope would be that predicted in eq. (3.11).

Anyway we remark that the instauration of this behaviour is very slow, as observed in our detailed model calculation. Thus we doubt that, e.g., in the experiments of ref. [10] the asymptotic surface tension dominated regime was tested.

We believe that the methods developed in this chapter allow investigation of other interesting issues, which could not be addressed here because of time limitations. Among this, we would like to mention the possibility of studying in our model further aspects related to the wetting phenomenology, e.g., the case of interaction potential ($\varepsilon/\alpha > 1$) which imply a nonzero T_w.

Another interesting problem, would be that of determining the trend of our $T_{c,n}$ in the limit of high coverage. In the case of flat substrates, it is known

that $T_{c,n} \underset{n\to\infty}{\to} T_R$, where T_R is the roughening temperature.[46] It would be interesting to establish a similar conclusion for the case of our fractal substrate.

A problem which we plan to undertake very soon is the application of our methods to the case of self–affine surfaces. This application requires a simple modification of the model. In this way we could possibly test the validity of the conclusions drawn in refs. [37] and [48] about the wetting of self–affine substrates in the high coverage regime.

PART TWO

CHAPTER 4

FRACTAL SURFACES, RANDOM WALKS AND SELF–AVOIDING WALKS

In the part one of this thesis we have shown how fractal geometry can be relevant for the description of phenomena like adsorption and wetting on rough substrates.

This does not exhaust the list of physical problems involving fractally rough surfaces. In this part of the thesis we address the problem of determining the spectral properties of a deterministic model of fractal surface. Such spectral properties are connected to those of diffusion on the same surface (see sect. 2.1). The interest of such calculations is at least twofold, in our opinion.

First of all, to our knowledge, the spectral and random walk dimensions of a fractal surface were never studied so far in a concrete model. The knowledge of the spectral dimension of a fractal surface allows also to solve a directly related problem in the conformational statistics of hierarchical polymeric networks, a subject which also attracted much attention recently.

Two subjects related to random walk (RW) diffusion, namely the random chain and the self–avoiding walk (SAW) problems, are also addressed in this part. Both this problems reveal interesting properties of the fractal structure studied, which could possibly be relevant in more general contexts.

4.1 SPECTRAL PROPERTIES OF FRACTAL SURFACES [49]

In many circumstances the description of processes occurring on fractal structures requires the knowledge of the spectral dimension, $\tilde{d}$,[12] besides the geometrical fractal dimension, $\bar{d}$. This is, e.g., the case of chemical reactions occurring on a self–similar surface, if particle diffusion is the controlling mechanism.[50] $\tilde{d}$ (see also sect. 2.1) is an intrinsic parameter characterizing the connectivity of a fractal structure, and is related by the equation $\tilde{d} = 2\bar{d}/d_w$ [12,13] to the fractal dimension $\bar{d}$. In this relation d_w is the dimension characterizing the long time behaviour of the average distance, $\langle R^2(t)\rangle^{1/2}$, travelled by a particle diffusing on the structure

$$\langle R^2(t)\rangle \underset{t\to\infty}{\sim} t^{2/d_w} \tag{4.1}$$

Furthermore $\tilde{d}$ characterizes the small frequency scaling behaviour of the density of harmonic (scalar) eigenmodes of the structure. A possible strategy for measuring $\tilde{d}$ for a fractal surface could be, e.g., inelastic neutron scattering.[14]

From a theoretical point of view the determination of $\tilde{d}$ for non–trivial fractal surfaces is an extremely hard task, especially if the structures are random. Even for deterministic fractals the only way to face this problem is numerical computation, unless particular ad hoc connectivities are assumed.[13] Here we address for the first time a numerical determination of $\tilde{d}$ for a non–trivial, deterministic model of a fractal surface.

4.1.1 *THE PROBLEM*

Fig. 4.1*a*) gives a sketch of the surface, on which we performed our Monte Carlo calculation, with its recursive construction rule. Since the number of elementary plaquettes increases by a factor 13 when the linear size is multiplied by 3, the fractal dimension is $\bar{d} = \ln 13/\ln 3 = 2.3347....$ We studied diffusion of a particle hopping between nearest neighbour sites on the network representing the surface.(*) At each time t ($t = 0, 1, 2, ...$) the particle resides on a site x and

(*) Since the surface has points which are overlapping we conventionally assume that these points are distinct and disconnected on the network, so that no jumps can occur between them.

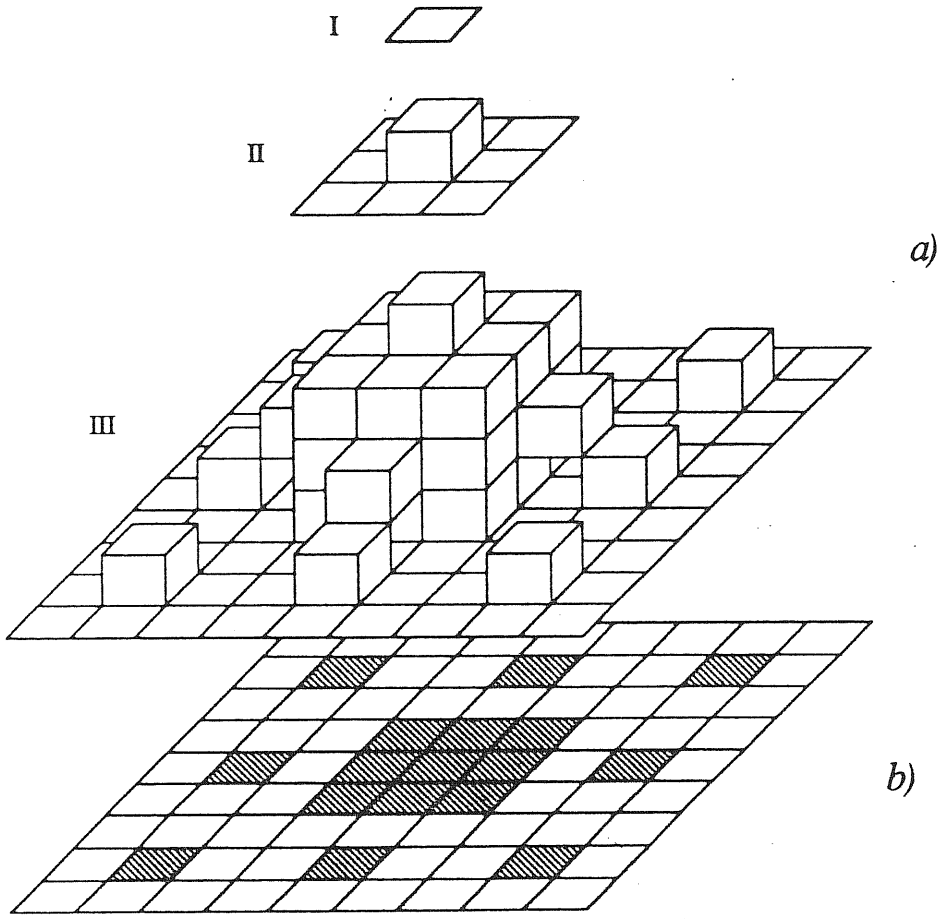

Fig. 4.1 "Hydrant" fractal surface. The surface is obtained by making use of the iterative construction scheme sketched in *a*). I, II and III are the first three steps of the construction. *b*) represents the basal plane of the hydrant at the third step: the dashed regions correspond to the bases of the buildings.

chooses, with equal probability, which of the n.n. sites will be occupied at time $t+1$ (miopic ant). By computing $\langle R^2(t)\rangle$ one can obtain an estimate for d_w, and thus $\tilde{d}$. Alternatively one can look at the asymptotic behaviour of $P_0(t)$, the probability that the particle is back at the starting point, 0, at time t.(**) This quantity is expected to scale like[12,13]

$$P_0(t) \sim \begin{cases} 1/[\langle R^2(t)\rangle]^{\tilde{d}/2} \sim t^{-\tilde{d}/2} & (\tilde{d} \leq 2) \\ t^{-1} & (\tilde{d} > 2) \end{cases} \tag{4.2}$$

(**) When computing $P_0(t)$ or $\langle R^2(t)\rangle$ we always perform averages with respect to many different starting points on the network.

for long times.

4.1.2 *COMPUTATIONAL TOOLS*

From a computational point of view, the main difficulty in a Monte Carlo analysis of RWs on a surface is the necessity of storing a large number of site positions and of connections of the sites with their neighbours. Indeed, one needs to make long walks on the structure in order to extract the asymptotic behaviour of the connected quantities.

To avoid the problems related to the use of a large amount of stored data, we devised an algorithm optimally exploiting the hierarchical properties of the surface. The algorithm, written in C language, is based on a recursive scheme. It calculates the positions of the surface points and of those connected to them while the walks are performed. In principle, the algorithm allows the construction of walks of any length. Due to its recursive nature, in fact, one can operate in any part of the surface without the necessity to store the positions of the sites previously explored by the walk. This feature completely avoids any limitation on the walks with the consequent finite size effects.

The calculations were done with a VAX Station 2000. The algorithm was particularly efficient especially for the calculation of quantities like $P_0(t)$. E.g., in the case of RWs on the between plaquette centers of the hydrant (see Fig. 4.1), performance of 10^6 RWs each 1000 steps long takes about 4000 secs CPU time. The calculation of $\langle R^2(t)\rangle$ in the same case, or in the case of walks between the network sites (see Fig. 4.1) is more time consuming.

4.1.3 *RESULTS AND DISCUSSION*

Fig. 4.2 and 4.3 report our numerical results for $\langle R^2(t)\rangle$ and $P_0(t)$, respectively, for walks of up to thousand steps. A best log–log fit for $\langle R^2(t)\rangle$ yields $d_w = 2.353 \pm 0.027$ when one considers diffusion between n.n. network sites (see Fig. 4.1a)), while $d_w = 2.332 \pm 0.032$ for diffusion between the centers of n.n. plaquettes (i.e. plaquettes having a common edge in Fig. 4.1a)). The evaluation of $P_0(t)$ for diffusion between plaquette centers gives $\tilde{d} = 2.005 \pm 0.031$ (see Fig.

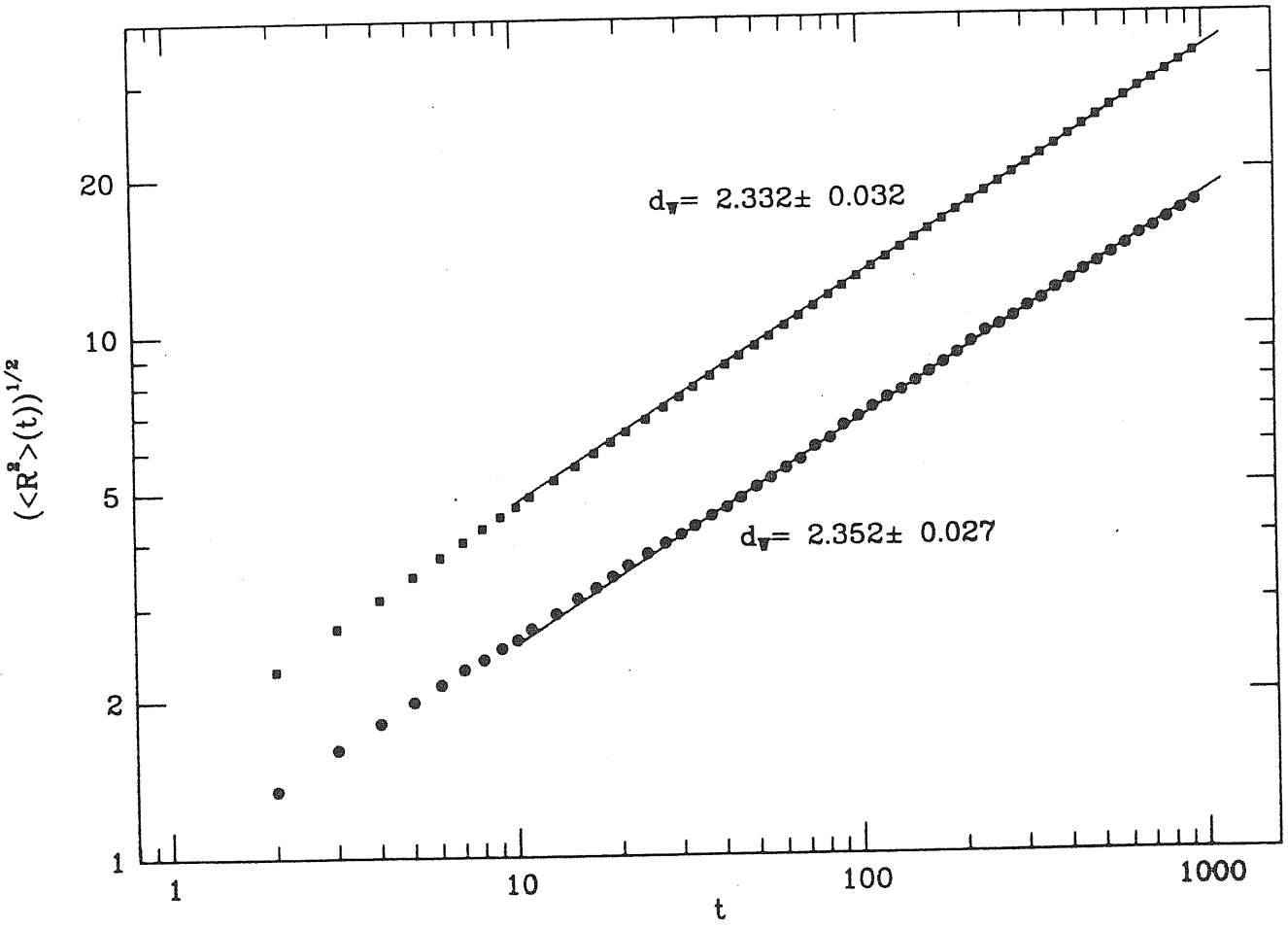

Fig. 4.2 Log–log plot of $(\langle R^2(t)\rangle)^{1/2}$ versus t for RWs on the hydrant surface. Full circles represent the average end–to–end distance for diffusion between n.n. sites of the network representing the surface (see Fig. 4.1a)). Full squares represent the same quantity (multiplied by 2 for convenience) for diffusion between the centers of n.n. plaquettes. Averages were calculated over 2×10^4 walks.

4.3).

Another quantity we computed is $S(t)$, the average number of distinct sites visited by a walk of t steps. This quantity is expected to scale asymptotically like $P_0(t)^{-1}$.[12,13] Numerical results were consistent with this scaling, but manifested a slower convergence to the asymptotic behaviour, than in the case of $P_0(t)$. This slower convergence is due to stronger scaling correction.

The fact that, within the errors, $\tilde{d} = 2$, shows that the hierarchical connectivity of the sites in Fig. 4.1a) is not able to modify the asymptotic scaling of the spectral properties with respect to the case of a regular, two–dimensional network.

Even if the surface in Fig. 4.1*a*) is topologically two–dimensional, the network representing it is hierarchical and irregular, and has even non–uniform coordination. This last feature is not present if we consider the network of diffusion sites when diffusion itself takes place between the plaquette centers. In this latter case the network is uniformly coordinated, but still hierarchical.

The above results and the considerations of the following section lead us to expect $\tilde{d} = 2$ also for surfaces having a $\bar{d}$ lower than that in Fig. 4.1*a*), and obtained with similar recursion schemes (e.g., one could consider a scheme in which each elementary plaquette grows into a square of 5×5 plaquettes, with the central one replaced by the lateral and upper sides of an elementary cube sitting on it, etc...). Such surfaces, as indicated by their $\bar{d}$, represent less pronounced deviations from the regular, flat plane situation. Within this construction scheme the example we considered is the one leading to the maximal $\bar{d}$, if one wants to avoid unphysical overlaps of different portions of the structure.

Of course, by making use, e.g., of triangular rather than square plaquettes, one could easily realize similar iterative constructions, leading to surfaces with even higher values of $\bar{d}$. Also on the basis of the arguments given below, we expect for all these generalizations $\tilde{d} = 2$.

The models we considered here can be conceived as well representative of situations in which the surfaces are moderately corrugated and clearly delimit two bulk regions both having the ordinary Euclidean dimension of the embedding space ("fat fractals").[51]

4.1.4 *A SCALING ARGUMENT*

Even if it is not possible to establish exactly that $\tilde{d} = 2$ for our surfaces, it is instructive to reinterpret our numerical results in the light of some scaling ideas which recently revealed very useful in problems of diffusion in inhomogeneous, hierarchical environments. Consider, e.g., a particle diffusing on a planar lattice. Let us assume that at each site x of the plane the particle can have a waiting time, i.e., it can take on average a certain time, τ_x, for the particle to actually perform a step (we can say $\tau_x \equiv 1$ in the models considered so far). If the τ's are distributed according to some fractal law in the plane, we should have $\tau(L) \sim \sum_{x \in \Lambda} \tau_x \sim L^{d_\tau}$,

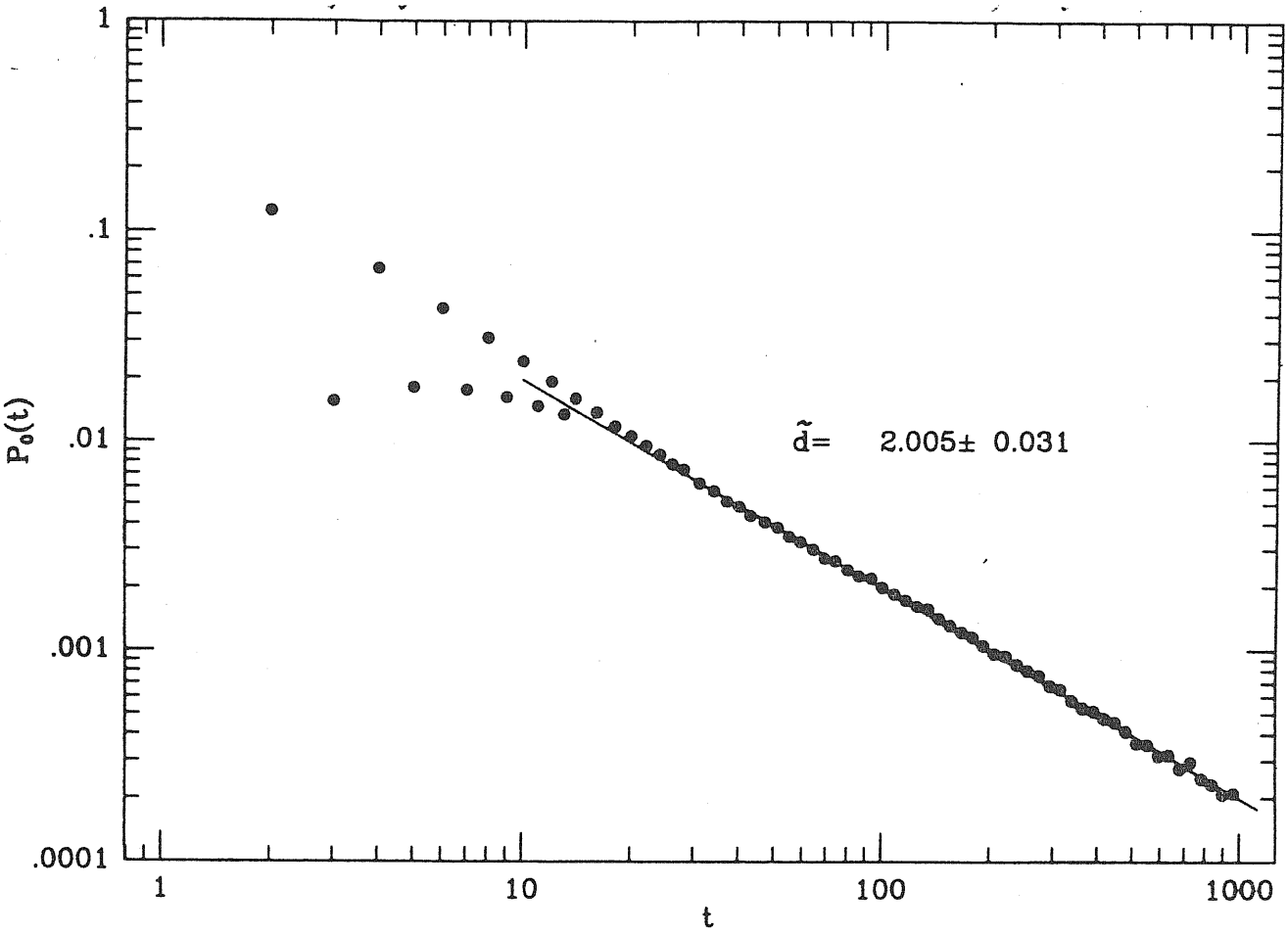

Fig. 4.3 Log–log plot of $P_0(t)$ versus t for diffusion between the centers of n.n. plaquettes of the hydrant surface. The data reported in the figure were evaluated for a set of 10^6 walks.

if Λ is a square region of size $L \times L$. d_τ is thus a fractal dimension associated to the waiting time distribution. Experience with exactly solvable diffusion problems shows that, in general, given a certain d_τ, the corresponding d_w of the diffusion with waiting times on a plane is correctly obtained by imposing [52,53]

$$\frac{t}{\left[\tau(\langle R^2\rangle^{1/2})/\langle R^2\rangle\right]} \sim \langle R^2\rangle \tag{4.3}$$

In other words, if the time unit is taken as the average waiting time per site in the visited region, the law of diffusion becomes normal. Taking into account the scaling of τ, and the fact that $t \sim \langle R^2\rangle^{d_w/2}$ (see eq. (4.1)), we obtain from eq. (4.3)

$$d_w = d_\tau \tag{4.4}$$

in this example. This is a particular case of a general scaling relation holding for diffusion with waiting times on a fractal structure[52,53]

Going back to our hydrant surface, the problem is thus to see what plays the role of $\tau(L)$ and what is d_τ. We can consider, as a sort of reference plane, the basal plane obtained at the n–th iteration of the construction procedure. On this plane the situation will look like that sketched in Fig. 4.1*b*), where the dashed regions corresponds to the bases of the "buildings" of different sizes obtained in the hydrant construction. We now imagine to describe the diffusion on the surface with reference to the basal plane, by saying that the particle is on a point in the white region when it is actually on the plane, or in a point of the dashed region, when it is wandering in the corresponding building. It is thus tempting to look at the dashed regions on the plane as to regions where a waiting time, proportional to the number of network points in the corresponding building, is shared. Since this number, for an $L \times L$ dashed square is proportional to $L^{\bar{d}}$, we conclude that, according to the above picture, $d_\tau = \bar{d}$.

By applying the result of eq.(4.4) to this sort of projected diffusion with waiting times, we finally get $d_w = \bar{d}$, which is what one finds numerically. It is important to notice that for analogous deterministic fractal models of branched polymers, e.g., the T–fractals,[54] arguments similar to those above lead to the exact result. Of course, in spite of its success, this relatively simple argument calls our attention on the need of a better theoretical understanding of the whole issue. In particular, a more rigorous meaning should be given to the intuitive idea of the "projected" motion.

4.2 IMPLICATIONS FOR THE STATISTICS OF POLYMERIC NETWORKS

The result for $\tilde{d}$ obtained in the previous section is somewhat unexpected. Our surfaces are networks with fully self–similar, hierarchical connectivity. For structures of this kind one could have expected $\tilde{d} \neq 2$.[55,56] On the other hand, the spectral properties of a network like the one studied here (see Fig. 4.1*a*)), are connected with the conformational statistics, in d dimensional Euclidean space, of

a phantom polymeric network with the same connectivity, as studied, e.g., in refs. [55], [56] and [57].

Indeed imagine, e.g., that the points $i, j, \ldots$ belong to a $d = 2$ network with regular (triangular) connectivity. Each point k of the network is then mapped into a point $\mathbf{x}_k \in R^d$. The problem is then to compute the conformational statistical properties of the image network in R^d, subject to an Hamiltonian of the form

$$H = K \sum_{\langle ij \rangle} (\mathbf{x}_i - \mathbf{x}_j)^2 \tag{4.5}$$

where $\langle \ldots \rangle$ denotes nearest–neighbors on the network.

Due to the Gaussian nature of the Hamiltonian, it is possible to establish a connection between the above conformational problem and the conduction properties of a resistor network with the same structure as that considered above, and with bond resistances $\propto 1/K$. E.g., the probability density that $\mathbf{x}_i - \mathbf{x}_j = \mathbf{R}$ is given by [58]

$$\begin{aligned} P_{ij}(\mathbf{R}) &= \frac{\prod_k \int d^d x_k \delta(\mathbf{x}_i - \mathbf{x}_j - \mathbf{R}) e^{-\beta H}}{\prod_k \int d^d x_k e^{-\beta H}} \\ &= \langle \delta(\mathbf{x}_i - \mathbf{x}_j - \mathbf{R}) \rangle = A e^{-\mathbf{R}^2/\Omega_{ij}} \end{aligned} \tag{4.6}$$

where $\beta = 1/k_B T$, Ω_{ij} is the resistance between points i and j. This last equation implies that

$$\langle (\mathbf{x}_i - \mathbf{x}_j)^2 \rangle \sim \Omega_{ij}. \tag{4.7}$$

In the case of the triangular network of the example, we clearly have

$$\Omega_{ij} \underset{|i-j| \to \infty}{\sim} \ln |i - j|, \tag{4.8}$$

which implies that the radius of gyration scales also logarithmically

$$\xi^2 = \tfrac{1}{2L} \textstyle\sum_{i,j} \langle (\mathbf{x}_i - \mathbf{x}_j)^2 \rangle \underset{L \to \infty}{\sim} \ln L. \tag{4.9}$$

If we now consider the case of a network with the connectivity of our hydrant surface (see Fig. 4.1), to determin Ω, and this ξ^2, we can exploit the connection between DC conduction problem and diffusion on the network. This link is provided by the Einstein relation. [59] If we indicate by ζ the resistance exponent (the

resistance between two points on the network at distance L scales as L^{ζ}), in a fractal structure one has [59]

$$\zeta = d_w - \bar{d} \tag{4.10}$$

where d_w is the RW dimension in the network and $\bar{d}$ is the network fractal dimension. In our present example, of course, $d_w = \bar{d} = 2$. On the other hand, the results for d_w obtained in our hierarchical surface imply that a network with the hierarchical connectivity of our surface (Fig. 4.1), when mapped in R^d, becomes a polymeric network again with

$$\xi \underset{L\to\infty}{\sim} \ln L \tag{4.11}$$

In other words, the hierarchical character of the connectivity is not sufficient to change the logarithmic behaviour ($\nu = 0$) into a power law one, as speculated in ref. [55] Apparently the only way to get deviations from the result $\nu = 0$ is that proposed in ref. [58], where a hierarchy in strength of the bonds in the network was considered.

4.3 THE RANDOM CHAIN

Another interesting issue which can be fruitfully addressed with our model calculation is that of the possible difference between the scaling properties of the diffusion problem and those of what could be defined as random chain problem. [60] By the latter we mean the statistics of the conformations of a random chain made of n.n. links of the network. Clearly, if the coordination number of the sites in the structure is not homogeneous, the statistics of RWs and random chain do not coincide. Even if the possible configurations of a diffusion path in time t, and of a random chain with t segments, are the same, they are not weighted equally. For the random chain the weight of each configuration is the same, while, for diffusion, the weight (or probability) of a given path depends on the coordinations of the visited points. A given diffusion path has a statistical weight equal to $\prod_x (1/z_x)$, where z_x is the coordination of site x and the product extends to the t initial sites of the walk steps. If z_x depends on x, like in our case, the weight depends on the walk considered, at variance with the random chain case.

To test whether such a different weight also implies a difference in the exponents describing the end–to–end distance in the two problems is an interesting question (for the random chain problem the end–to–end distance exponent, d_c, corresponds to d_w and is the reciprocal of the ν exponent in polymer statistics language).

When dealing with fractals with inhomogeneous coordinations one can find that random chain and RW diffusion problems have very different behaviours.[60,61] For some deterministic fractal networks one has even found that d_w is finite, while $d_c = \infty$ (logarithmic behavior of $\langle R^2 \rangle^{1/2}$ as a function of chain length).[60]

We performed with our methods an extensive simulation of the random chain problem. Our results, surprisingly enough, indicated a possible coincidence of d_c with d_w, at variance with the above mentioned cases. Indeed we found $d_c = 2.345 \pm 0.034$ which is very close to the estimate for d_w. This finding calls attention on the need of a deeper understanding of the physical mechanisms possibly leading to $d_c \neq d_w$ in a specific problem.

As to the possible practical implications of the result for d_c, it is worth noticing that an interesting interpretation of the random chain problem is in terms of diffusion in the presence of traps which possibly annihilate the walking particle. These traps are located at each site x with coordination $z_x < z_{max}$, where z_{max} is the maximal coordination in the network (5 in the case of the hydrant surface). On these sites the probability of trapping for the particle is $(z_{max} - z_x)/z_{max}$, so that the probability of a walk of t steps has the form

$$\prod_x \left(\frac{z_x}{z_{max}}\right)\left(\frac{1}{z_x}\right) = \left(\frac{1}{z_{max}}\right)^t , \tag{4.12}$$

z_x/z_{max} being the probability that the particle is not trapped at site x. Our d_c is thus characterizing the asymptotic time dependence of the average distance travelled by particles which are not annihilated by the traps up to time t.

To test whether in fractal structures $d_c = d_w$, or not, is of much importance, e.g., for establishing Flory approximations to the problem of SAWs on these structures. Indeed all Flory formulas proposed so far for SAWs on fractal structures are based on a dynamical picture of the walks in both the non–interacting and interacting regimes. Thanks to this dynamical description, these formulas connect the fractal dimension of the SAWs to the $\bar{d}$ and the d_w (or $\tilde{d}$) of the structure.

Since the SAW problem is in principle a static problem (conformations of a self–repelling chain), it is not obvious, a priori, that this dynamical interpretation is legitimate. It is indeed somewhat surprising that so little attention was paid to this problem in the recent literature.

A possible way out for the validity of the above Flory approaches opens when dynamical diffusion has the same dimension as the static random chain problem on the structure. This is certainly always the case when dealing with fractal structures with homogeneous coordination (like for the Sierpinski Gasket, see sect. 2.1), but is not necessarily true in general.

It is remarkable that in our hydrant surface, which has no uniform coordination, $d_c = d_w$. This fact makes us confident that a Flory approach to the SAW problem, based on a dynamical picture, could be meaningful and successful for the case of our surface. We show that this is indeed the case in the next section.

4.4 SELF–AVOIDING WALKS

The results reported in the previous sections strongly support the validity, for a fractal surface, of the two relations: $\tilde{d} = 2$ (i.e., $d_w = \bar{d}$) and $d_c = d_w$. These facts, also in the light of the last considerations in the previous section, led us to consider also the problem of SAWs on our surface. This calculation can also be relevant in connection with possible applications to the study of conformations of polymers adsorbed on self–similar surfaces.

We performed a Monte Carlo calculation of the end–to–end distance of SAWs by two different methods. SAWs were generated by a simple–sampling (SS) as well as a biased[62] (BS) method. Best log–log fits for the $\langle R^2_{SAW}(t)\rangle$ obtained in the two cases (see Fig. 4.4) gave respectively the following values for the SAW fractal dimension: $d^{(SS)}_{SAW} = 1.5243 \pm 0.035$ and $d^{(BS)}_{SAW} = 1.5216 \pm 0.025$. Within the numerical errors, the two estimates of d_{SAW} are clearly compatible.

Since $d_c = d_w$ in our case, it legitimate to use Flory arguments for the determination of d_{SAW}. A possible Flory approach to the calculation of the fractal dimension of SAWs[63] is based on the minimization of the total free energy function constituted by a repulsive energy term (due to self–avoidance) and an entropic

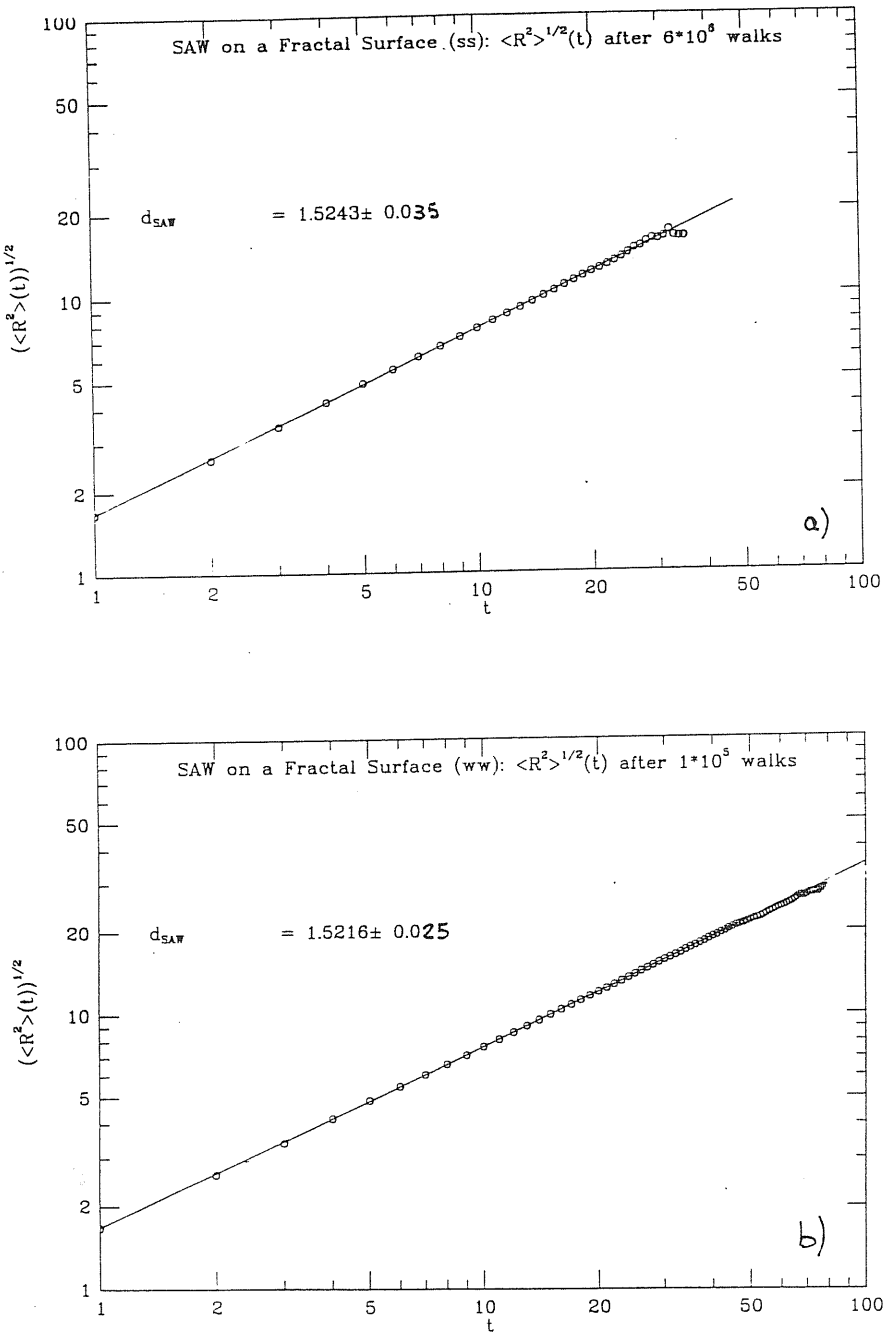

Fig. 4.4 Log–log plot of $(\langle R^2_{SAW}(t)\rangle)^{1/2}$ versus t for the SAWs on the hydrant surface. *a*) simple sampling method; *b*) biased sampling method.

term. In a fractal structure it is natural to accept that the repulsive energy term should be estimated as $\sim N^2/R^{\bar{d}}_{SAW}$, where N is the number of steps, R_{SAW} the elongation of the SAW, and $\bar{d}$ the fractal dimension of the structure where SAWs are performed. Less obvious is the choice of the entropic term. The crucial

question is whether one can assume a purely Gaussian distribution for the end–to–end elongation of a RW on a fractal structure, or not. In spite of the fact that, a stretched Gaussian rather that a Gaussian distribution should be expected for RWs on fractals, Flory results obtained by the former distribution are often not very satisfactory.[64] Dekeyser *et al.*,[63] proposed that the entropic term should should scale as $\sim R_{SAW}^2/L^{2/d_w}$ as implied by a Gaussian distribution. A justification for such an apparently inconsistent choice, can be found both in the soundness of the results,[63,65] and in the fact that Flory approximations are in general expected to realize a balance between presumably big errors in both energy and entropy estimates. So the Flory free energy will have the form

$$F = a\frac{N^2}{R_{SAW}^{\bar{d}}} + b\frac{R_{SAW}^2}{N^{2/d_w}}. \tag{4.13}$$

The extremalization of this expression gives[63]

$$R_{SAW} \sim N^{\frac{2+\bar{d}}{2(1+d_w^{-1})}}, \tag{4.14}$$

i.e.

$$d_{SAW} = \frac{2+\bar{d}}{2(1+d_w^{-1})}. \tag{4.15}$$

Recent investigations have shown that eq. (4.15) qualifies as an optimal approximation among several others which have been proposed for deterministic and random fractal structures.[65]

Taking into account the results reported in the previous sections, we would thus expect that, on the basis of (4.15) $d_{SAW} = (2+\bar{d})/2(1+\bar{d}^{-1}) = 1.5174\ldots$ (remember that $\bar{d} = \ln 13/\ln 3$ for our fractal surface). Remarkably enough, this value of d_{SAW} agrees, within the numerical errors, with the values obtained by our simulations.

Of course, the success of eq. (4.15) in this example could be just fortuitous. Also the coincidence of d_c and d_w, as a rule, is not at all guarantee of striking success for Flory approximations of the type discussed above. We mentioned here the results mostly in order to call attention on the general problem, of the foundation of the Flory approach to SAWs on fractals. Any derivations of Flory formulas in this context should preliminarly address the issue of whether it is legitimate, or not, to consider the problem as a dynamical one.

4.5 CONCLUSIONS

Summarizing, in this chapter we have presented a model calculation clearly indicating that diffusion on some deterministic fractal surfaces can be characterized by $d_w = \bar{d}$ and thus $\tilde{d} = 2$. It is conceivable that such result could hold also in the case of random fractal surface models, much less accessible to numerical investigations. This $\tilde{d}$ is consistent with an interpretation in terms of scaling laws governing diffusion with a fractal distribution of waiting times.

While on the basis of our model results we can expect $d_w = \bar{d}$ in a wide class of surface problems, characterized by the fact that the surface itself delimits fat fractal regions, the problem of establishing more precisely the limits of validity of $\tilde{d} = 2$ remains open.

The fact that $\tilde{d} = 2$ for a fractal surface has interesting implications for the statistics of polymeric networks. Indeed, at least in the example discussed here, we were able to conclude that a hierarchical connectivity is not able to alter the scaling properties of a polymeric network, with respect to those of the regular network case.

On the basis of this last result, it is also conceivable, that the introduction of self–avoidance for the networks would not lead to different exponents in the regular and hierarchical cases. This, e.g., would be guaranteed within a Flory approach like that developed in refs. [57] and [58].

We also verified that for our model surface, within the uncertainties, $d_c = d_w$, unlike in other fractal structures. This circumstance is an important requisite for the application of dynamically based Flory arguments. We gave an example of how such an argument can work well in the study of SAWs on our hydrant surface.

We are well aware that interesting issues concerning walks in the presence of fractal surfaces were not covered by this thesis.

Among them we would like to cite the problem of surface entropic exponents for SAWs, when the surface is fractal and bulk is three dimensional. The entropic surface exponent γ_1 characterizes the asymptotic behaviour of the number of SAWs starting from a point near a boundary, and never trespassing it. This number is

given by

$$C_N^{'} \propto N^{\gamma_1 - 1} K_c^{-N}, \tag{4.16}$$

K_c being the critical step fugacity.

Studies of γ_1 for fractal boundaries in two dimensional bulk have revealed extremely remarkable universalities for the surface magnetic exponent with different boundaries.[66] An extension of such investigations to the $d = 3$ case would certainly be very welcome. We did not address this issue here, because of time limitations, and because it would require a considerable further investment of computational power. However, the algorithms used for the calculations in this chapter are certainly a very promising starting point for an attack of this problem.

BIBLIOGRAPHY

[1] B.B.Mandelbrot, *"The Fractal Geometry of Nature"*, San Francisco, W.H.Freeman (1982).

[2] P.G.de Gennes, *"Scaling Concepts in Polymer Physics"*, Cornell Univ. Press, Ithaca (1979).

[3] *"On Growth and Form"*, edited by H.F.Stanley and N.Ostrowsky, NATO ASI Ser. Vol 100 (Nijhoff, Dordrecht, 1986).

[4] R.Serra, M.Andreatta, M.Compiani and G.Zanarini, *"Introduction to Physics of Complex Systems"*, Pergamon Press, 1986.

[5] H.J.Stapleton, J.P.Allen, C.P.Flynn, D.G.Stinson and S.R.Kurtz, *Phys. Rev. Lett.* **45**, 1456 (1980).

[6] M.Mezard, G.Parisi, N.Sourlas, G.Toulouse and M.Virasoro, *Phys. Rev. Lett.* **52**, 1156 (1984).

[7] S. Dietrich, in *"Phase Transition and Critical Phenomena"*, Vol. 12, by C.Domb and J.L.Lebowitz, Academic Press (1985), pp.1–218.

[8] D.Avnir, D.Farin and P.Pfeifer, *NATURE* **308**, 261 (1984).

[9] P.G.de Gennes, in *"Physics of Disordered Materials"*, by D.Adler, H.Fritzsche and S.R.Ovshinsky, Plenum Press, New York (1985), pp.227–241.

[10] P.Pfeifer, Y.J.Wu, M.W.Cole and J.Krim, *Phys. Rev. Lett.* **62**, 1997 (1989).

[11] P.Pfeifer, J.Kenntner and M.W.Cole, in *Proc. of Conf. "Fundamentals of Adsorption"*, edited by A.Nersmann (1989).

[12] S.Alexander and R.Orbach, *J. Phys.(Paris) Lett.* **43**, L625 (1982).

[13] R.Rammal and G.Toulouse, *J. Phys.(Paris) Lett.* **44**, L13 (1983).

[14] P.Pfeifer, A.L.Stella, F.Toigo and M.W.Cole, *Europhys. Lett.* **3**, 717 (1987).

[15] D.A.Huse, *Phys. Rev. B* **30**, 1371 (1984).

[16] M.P.Nightingale, W.F.Saam and M.Schick, *Phys. Rev. B* **30**, 3830 (1984).

[17] R.Pandit, M.Schick and M.Wortis, *Phys. Rev. B* **26**, 5112 (1982).

[18] C.Ebner, C.Rottmann and M.Wortis, *Phys. Rev. B* **28**, 4186 (1983).

[19] C.Ebner, *Phys. Rev. B* **28**, 2890 (1983).

[20] J.Krim, J.G.Dash and J.Suzanne, *Phys. Rev. Lett.* **52**, 640 (1984).

[21] M.J.de Oliveira and R.B.Griffihs, *Surface Science* **71**, 687 (1978).

[22] C.Ebner, *Phys. Rev. A* **22**, 2776 (1980).

[23] R.Evans and P.Tarazona, *J. Chem. Phys.* **80**, 587 (1984).

[24] R.E.Benner, L.E.Scriven and H.T.Davis, *Faraday Symp. Chem. Soc.* **16**, 169 (1983).

[25] R.E.Benner, G.F.Teletzke, G.F.Scriven and H.T.Davis, *J. Chem. Phys.* **80**, 589 (1981).

[26] R.Lipowsky, *Z. Phys. B* **55**, 345 (1984).

[27] S.Gregg and K.S.W.Sing, *"Adsorption, Surface Area and Porosity"*, San Francisco, W.H.Freeman (1982).

[28] R.Evans, U.M.B.Marconi and P.Tarazona, *J. Chem. Phys.* **84**, 2376 (1986).

[29] B.Derjaguin, *Acta Physicochimica URSS* **12**, 181 (1940).

[30] R.Evans and U.M.B.Marconi, *Chem. Phys. Lett.* **114**, 415 (1985).

[31] D.H.Everett and J.M.Haynes, in *"Colloid Science"*, Vol.1, Specialist Periodicals Reports (D.H.Everett and H.Douglas, eds.), p. 123. Chemical Society, London.

[32] D.Avnir and M.Jaroniec, *LANGMUIR* **5**, 1431 (1989).

[33] P.Pfeifer, U.Welz and H.Wippermann, *Chem. Phys. Lett.* **113**, 535 (1985).

[34] B.Nienhuis, *Phys. Rev. Lett.* **49**, 1063 (1982).

[35] P.G.de Gennes, *La Reserche* **7**, 919 (1976).

[36] A.Maritan and A.Stella, *Phys. Rev. B* **34**, 456 (1986).

[37] M.Kardar and J.O.Indekeu, *Europhys. Lett.* **12**, 161 (1990).

[38] J.Krim and V.Panella, *Preprint* (1990).

[39] P.Pfeifer, M.Obert and M.W.Cole, *Proc. R. Soc. Lond. A* **423**, 169 (1989).

[40] J.Frenkel, *"Kinetic Theory od Liquids"*, Oxford University Press, London and New York, 1946.

[41] G.J.Halsey, *J. Chem. Phys.* **16**, 1931 (1948).

[42] T.L.Hill, *J. Chem. Phys.* **15**, 767 (1947).

[43] R.Lipowsky and M.E.Fisher, *Phys. Rev. Lett.* **56**, 472 (1986).

[44] G.Giugliarelli and A.L.Stella, *Physica Scripta* (1990) in press.

[45] E.Cheng, M.W.Cole and A.L.Stella, *Europhys. Lett.* **8**, 537 (1989).

[46] C.Ebner, *Phys. Rev. A* **23**, 1925 (1981).

[47] G.Giugliarelli and A.L.Stella, in preparation.

[48] M.Kardar and J.O.Indekeu, *Phys. Rev. Lett.* **65**, 662 (1990).

[49] G.Giugliarelli, A.Maritan and A.L.Stella, *Europhys. Lett.* **11**, 101–106 (1990).

[50] J.Klafter, G.Zumofen and A.Blumen, *Phys. Rev.* **B28**, 6112 (1983).

[51] C.Grebogi, S.McDonald, E.Ott and J.A.Yorke, *Phys. Lett.* **A110**, 1 (1985).

[52] J.Machta, *J. Phys.* **A18**, L531 (1985).

[53] S.Robillard and A.M.Tremblay, *J. Phys. France* **A19**, 2171 (1986).

[54] S.Havlin and D.Ben–Havraham, *Advances in Physics* **36**, 695 (1987).

[55] M.E.Cates, *Phys. Rev. Lett.* **53**, 926 (1984).

[56] M.E.Cates, *Phys. Lett.* **161B**, 363 (1985).

[57] Y.Kantor, M.Kardar and D.R.Nelson, *Phys. Rev. Lett.* **57**, 791 (1986).

[58] A.Maritan and A.L.Stella, *Phys. Rev. Lett.* **59**, 300 (1987).

[59] Y.Gefen, A.Aharony and S.Alexander, *Phys. Rev. Lett.* **50**, 77 (1983).

[60] A.Maritan, *Phys. Rev. Lett.* **62**, 2845 (1989).

[61] C.Vanderzande, unpublished 1989.

[62] M.N.Rosenbluth and A.W.Rosenbluth, *J. Chem. Phys.* **23**, 356 (1955).

[63] R.Dekeyser, A.Maritan and A.Stella, *Phys. Rev. A* **36**, 2338 (1987).

[64] R.Rammal, G.Toulouse and J.Vannimenus, *J. Phys. (Paris)* **48**, 389 (1984).

[65] S.L.A. de Queiroz, F.Seno and A.L.Stella, *Preprint* (1990).

[66] A.L.Stella and C.Vanderzande, *Int. J. Mod. Phys.* **4**, 1437 (1990).

ACKNOWLEDGEMENTS

First of all I would like to thank Prof. Attilio L. Stella for his continuous support during the thesis and for having initiated me in this field. I'm also grateful to Dr. Franca Aicardi for her help in the developing of the algorithm to perform random walks on the hydrant surface. I would like to thank also Prof. A. Borsellino for giving me the opportunity to work through these years in the Biophysics Sector of the International School of Advanced Studies in Trieste.